STEM CELLS

Lung cell transplantation for pulmonary fibrosis

Irit Milman Krentsis[1]†, Yangxi Zheng[1]†, Chava Rosen[1,2], Sarah Y. Shin[3], Christa Blagdon[1], Einav Shoshan[1], Yuan Qi[4], Jing Wang[4], Sandeep K. Yadav[1], Esther Bachar Lustig[1], Elias Shetzen[1], Burton F. Dickey[5], Harry Karmouty-Quintana[3,6], Yair Reisner[1]*

Idiopathic pulmonary fibrosis is a major cause of death with few treatment options. Here, we demonstrate the therapeutic efficacy for lung fibrosis of adult lung cell transplantation using a single-cell suspension of the entire lung in two distinct mouse systems: bleomycin treatment and mice lacking telomeric repeat-binding factor 1 expression in alveolar type 2 (AT2) cells (*SPC-Cre TRF1$^{fl/fl}$*), spontaneously developing fibrosis. In both models, the progression of fibrosis was associated with reduced levels of host lung progenitors, enabling engraftment of donor progenitors without any additional conditioning, in contrast to our previous studies. Two months after transplantation, engrafted progenitors expanded to form numerous donor-derived patches comprising AT1 and AT2 alveolar cells, as well as donor-derived mesenchymal and endothelial cells. This lung chimerism was associated with attenuation of fibrosis, as demonstrated histologically, biochemically, by computed tomography imaging, and by lung function measurements. Our study provides a strong rationale for the treatment of lung fibrosis using lung cell transplantation.

INTRODUCTION

Idiopathic pulmonary fibrosis (IPF) has an estimated prevalence of 13 to 20 per 100,000 people worldwide. About 100,000 people are affected in the United States, and 30,000 to 40,000 new cases are diagnosed each year (World Health Organization) (*1*–*4*). Prognosis in IPF remains poor, with a median survival of 3.5 years (*5*–*8*) from the time of diagnosis, in adults aged 65 years or older. IPF is characterized by a typical interstitial pneumonia pattern on high-resolution computed tomography (CT) scanning, as manifested by basal predominant reticulation, traction bronchiectasis, and honeycombing (*5*, *9*–*14*). Although the antifibrotic drugs pirfenidone (*6*, *7*, *15*–*18*) and nintedanib (*19*–*22*) can slow disease progression to some extent, the only treatment with the proven capability to improve survival is lung transplantation (*23*). However, the shortage of lungs suitable for transplantation and the high procedure-related mortality risk have led to an extensive search for lung stem cell populations that could potentially offer alternative sources for transplantation and less invasive treatment (*24*–*32*).

Recently, we showed that transplantation of fetal (*33*) or adult (*34*) lung progenitors could potentially engraft and induce lung chimerism following naphthalene (NA) or cyclophosphamide-induced (CY) lung injury (*33*, *35*), provided that the lung stem cell niche in the recipient is vacated of endogenous lung progenitors by adequate conditioning. Following lung injury with NA or CY, the endogenous host lung progenitors, which are generally quiescent, exhibit a robust proliferative response, competing with donor progenitors, thereby preventing engraftment. However, these endogenous proliferating cells are radio-sensitive and can be eliminated by subsequent sublethal 6-gray (Gy) total body irradiation (TBI) (*33*). Thus, transplantation of fetal or adult lung cells following such conditioning leads to extensive donor-derived "patches," comprising bronchiolar, alveolar, and endothelial cell lineages, and to substantial improvement of lung function (*33*–*35*).

In the present study, we investigated the curative potential of this approach for lung fibrosis. To that end, we used two distinct mouse models: the bleomycin (BLM) chemical injury model (*36*) and the genetic *SPC-Cre TRF1$^{fl/fl}$* (*37*) model. BLM induces a fibrotic reaction in mice within a short period (typically 3 weeks after administration). It has often been observed that BLM-induced fibrosis is partially reversible, and therefore, its use was largely limited to short-term experiments assessing potential therapeutic agents within 4 to 5 weeks after completion of BLM administration. BLM is generally administered intratracheally (it) (*38*–*43*) using a single dose that produces a bronchiolocentric distribution of fibrosis. Alternatively, it can be administered intravenously (iv) (*44*, *45*) or intraperitoneally (ip) (*46*, *47*). Prolonged intraperitoneal administration of BLM was reported to be associated with a longer fibrosis period (*36*, *48*). In contrast, the *SPC-Cre TRF1$^{fl/fl}$* model (*37*), where lung fibrosis occurs spontaneously following tamoxifen (TMX) treatment, offers a more clinically relevant model of lung fibrosis considering the occurrence of shortening of telomeres and senescence of AT2 alveolar cells as has been implicated in patients with IPF (*11*, *49*).

In this model, deletion of telomeric repeat-binding factor 1 (Trf1) in surfactant protein C–positive (SPC$^+$) alveolar type 2 (AT2) cells leads to spontaneous fibrosis that progresses over a prolonged period, thereby allowing assessment of the role of lung stem cell transplantation at late time points after transplantation. Notably, in both the BLM and *SPC-Cre TRF1$^{fl/fl}$* models, we found that a minimal level of fibrosis correlates with effective engraftment of donor-derived patch-forming lung progenitors without the need for any additional conditioning. Furthermore, we demonstrate in the BLM model that this minimal level of fibrosis is associated with marked elimination of endogenous patch-forming cells, in line with our hypothesis that overcoming stem cell competition is a prerequisite for

[1]Department of Stem Cell Transplantation and Cell Therapy, MD Anderson Cancer Center, Houston, TX, USA. [2]Department of Neonatology, Edmond and Lily Safra Children's Hospital, Sheba Medical Center, Tel-Hashomer, Israel. [3]Department of Biochemistry and Molecular Biology, The University of Texas Health Science Center at Houston, Houston, TX, USA. [4]Department of Bioinformatics and Computational Biology, MD Anderson Cancer, Houston, TX, USA. [5]Department of Pulmonary Medicine, Division of Internal Medicine, The University of Texas MD Anderson Cancer Center, Houston, TX, USA. [6]Divisions of Critical Care, Pulmonary and Sleep Medicine, Department of Internal Medicine, The University of Texas Health Science Center at Houston, Houston, TX, USA.
*Corresponding author. Email: yreisner@mdanderson.org
†These authors contributed equally to this work.

effective engraftment. Last, upon effective chimerism induction, we demonstrate fibrosis attenuation and functional benefit in both models. These results offer proof of concept for clinical use of lung progenitor cell transplantation in patients with lung fibrosis.

RESULTS

Adaptation of a BLM mouse model for the evaluation of stem cell therapy

Lung fibrosis induced in several previously described BLM mouse models was shown to be reversible (*44*, *48*, *50*). It was therefore critical to develop a more enduring model to enable the assessment of lung stem cell transplantation efficacy, which requires a period of about 6 to 8 weeks after transplantation to arrest the deterioration of lung function (*33*, *34*). Thus, we adopted and optimized in the present study the protocol described by Headley *et al.* (*36*) making use of low-dose BLM administered systemically over a period of 4 weeks to induce more stable lung fibrosis, which enables the benefit of the transplanted cells to be assessed at relatively late time points following cell transfer.

As shown in Fig. 1, intraperitoneal administration of BLM for 4 weeks (total of eight doses each of 0.035 U/g) led to marked lung fibrosis, detected by CT (Fig. 1, A and B) and by the quantitative hydroxyproline assay for collagen levels at 8 weeks after completion of BLM treatment (Fig. 1C). Furthermore, substantial fibrosis was indicated by hematoxylin and eosin (Fig. 1D), trichrome (Fig. 1E and fig. S1, A and B), alpha–smooth muscle actin (α-SMA) (Fig. 1F and figs. S1C and S10A), fibronectin (Fig. 1G), collagen IV (Fig. 1H), and hyaluronic acid (HA) staining (fig. S10A). Notably, analysis of lung function parameters measured by FlexiVent at different time points after completion of BLM treatment revealed maximal loss of function at 6 to 8 weeks following completion of BLM administration (Fig. 1I). These results demonstrate that the BLM-induced lung damage is stable over a prolonged period, allowing the therapeutic effect of our suggested lung transplantation modality to be evaluated at 2 months after transplantation if performed after 4 weeks of BLM administration.

Depletion of endogenous patch-forming progenitor cells by BLM treatment

We previously demonstrated in NA- or CY-treated mice that engraftment and colonization of lung progenitors require subsequent conditioning treatment after 2 days with sublethal 6-Gy TBI (*33*–*35*). As shown by fluorescence-activated cell sorting (FACS) analysis, this transplant modality leads to robust lung chimerism at 6 months after transplant, exhibiting 48% donor-derived cells within the $CD45^-$ population (fig. S2, A and B). Single-cell RNA sequencing (scRNA-seq) analysis of sorted donor-derived $CD45^-$ lung cells (figs. S2, C to E, and S3, A to E) revealed a similar distribution of various cell types in this fraction compared to control-sorted $CD45^-$ lung cells from untreated normal mice (fig. S3, D and E). This similar distribution also revealed a reduced proportion of epithelial cells in all the samples, likely associated with a selective loss of these cells following the enzymatic process involved in the preparation of single-cell suspension (*51*). Notably, we previously demonstrated in this mouse model that the pretransplantation conditioning enables endogenous lung progenitors to be effectively vacated from their niches, thereby reducing stem cell competition between host and donor cells for these niches (*33*). Thus, we initially interrogated the impact of BLM treatment on endogenous patch-forming cells. To that end, we used our previously described transplantation assay in which recipient mice are conditioned by CY and 6-Gy TBI. C57BL/6-Tdtomato$^+$ [B6.129(Cg)-*Gt(ROSA)26Sor*$^{tm4(ACTB\text{-}tdTomato,\text{-}EGFP)Luo}$/J] and C57BL/6-GFP$^+$ [C57BL/6-Tg (CAG-EGFP)1Osb/J] mice (green fluorescent protein), used as donors, were treated with BLM for 1, 2, or 4 weeks, and thereafter, lung cells were harvested and transplanted in different doses (2×10^6, 4×10^6, or 8×10^6 cells) into recipient C57BL/6 mice conditioned with CY and 6-Gy TBI (Fig. 2A). Donor-derived patches were determined in recipient mice at 64 days after transplant. Considering that the TdTomato and GFP donor mice are congenic to the recipient animals and might be rejected to some extent, we used a 1:1 mixture of cells from both strains to ascertain that strong engraftment is exhibited after transplantation of lung cells from both types of donors. Also, because of the limited availability of fluorescent donor mice, this approach was useful for attaining the large number of fluorescent donor cells required for our extensive transplantation experiments. As shown in Fig. 2 (B and C), depicting typical immunohistology of donor-derived patches and quantitative analysis of patch number per 2-mm^2 lung tissue, respectively, high levels of patch-forming progenitors persisted in donor mice following BLM treatment for 1 to 2 weeks, while 4 weeks of BLM treatment markedly reduced the patch-forming lung cells. These results strongly suggest that BLM treatment alone is associated with the loss of endogenous patch-forming lung progenitors and can make space for engraftment of donor-derived patch-forming cells when used in recipient animals.

Successful engraftment of donor-derived progenitor cells in the BLM mouse model without conditioning treatment

In line with the efficacy of progressive ablation of endogenous lung patch-forming cells by BLM, we found that transplantation of lung cells from TdTomato-positive donors into BLM-treated mice (Fig. 3A) failed to induce substantial levels of donor-derived lung patches following treatment of recipients for 1 to 2 weeks with BLM, while BLM treatment for 3 weeks led to partial chimerism, and treatment for 4 to 5 weeks enabled robust induction of donor-derived lung patches. This was shown by quantitative analysis of the number of donor-derived patches per 2-mm^2 lung area in the lungs of recipient mice (Fig. 3, B and C). In addition, the different levels of chimerism following transplantation after treatment with BLM for different time periods are illustrated in two mice from each group by views of large lung areas (Fig. 3D). Thus, following lung harvest and before fixation and freezing, the whole-lung tissue was imaged by immunofluorescence microscopy. Additional eight examples of such large views depicting the variability of chimerism among 20 mice transplanted after 4 weeks of BLM treatment are shown in fig. S4. These results strongly support the concept of stem cell competition, suggesting that the ablation of endogenous lung progenitors attained following BLM treatment for 4 to 5 weeks allows for effective engraftment and colonization of donor-derived lung patches without additional conditioning with TBI or other toxic agents.

Identification of donor-derived epithelial, endothelial, and mesenchymal cells in the BLM mouse model

Next, we identified by immunohistology the different cell types comprising the donor-derived patches following transplantation into mice treated with BLM for 4 weeks. In these experiments, GFP$^+$ donors were used for transplantation, and quantitative chimerism

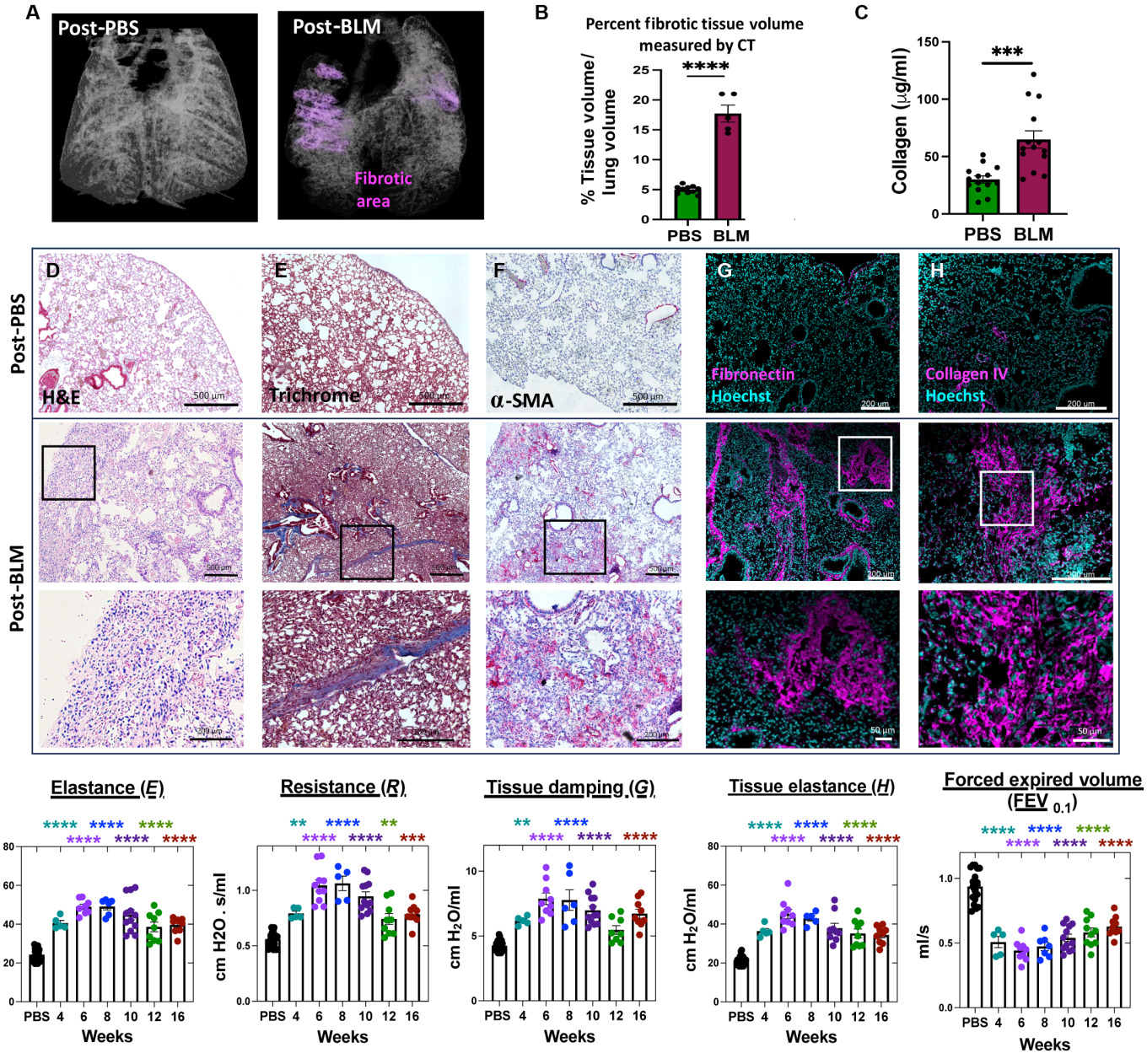

Fig. 1. Assessment of durable BLM-induced lung fibrosis. (**A**) Typical micro-CT 3D image of lung tissue from mice following treatment with phosphate-buffered saline (PBS; left) and at 8 weeks after completion of intraperitoneal BLM administration for 4 weeks (total of eight doses, of 0.035 U/g, each). Fibrotic tissue is indicated in purple. (**B**) Percent fibrotic tissue (tissue volume area divided by the total lung volume) was calculated on the basis of the micro-CT scans 8 weeks after completion of BLM treatment. (**C**) Quantitative determination of total collagen in the paraffin-embedded lung tissue measured by the hydroxyproline assay. (**D** to **H**) Representative lung staining 8 weeks after completion of BLM treatment (bottom rows) compared to treatment with PBS (top row). (D) Hematoxylin and eosin (H&E), (E) trichrome, (F) alpha–smooth muscle actin (α-SMA), (G) fibronectin, and (H) collagen IV staining. Scale bars, 500 µm (D to F, top and middle rows), 200 µm (D to F, bottom row), 200 µm (G and H, top and middle rows), and 50 µm (G and H, bottom row). (**I**) Lung function assessment measured by FlexiVent at different time points after completion of BLM treatments. Results were taken from one transplantation experiment. For the PBS control group and groups analyzed at 4, 6, 9, 10, 12, and 16 weeks of BLM treatment, $N = 18, 5, 9, 6, 11, 9$ and 10, respectively. One-way ANOVA with Dunnett's test was used in (I), and an unpaired *t* test was used in (B) and (C) for statistical analysis for comparison between BLM- and PBS-treated groups; $^{**}P < 0.002$, $^{***}P < 0.0002$, and $^{****}P < 0.0001$.

analysis was assessed at 8 weeks after transplant. To quantitate alveolar, endothelial, and mesenchymal cells, we used double staining for GFP and different cell markers for AT1 (AQP5), AT2 (LAMP3) endothelial cells (CD31), and mesenchymal cells (PDGFRα). Typical staining for donor-derived cells stained with each of these markers is illustrated in Fig. 4 and figs. S5 to S7. In addition, considering that endothelial and AT1 cells are relatively thin and can reside close to each other, we performed triple staining for GFP, AQP-5, and CD31 to affirm the reliability of our staining. A typical example of this staining, shown in fig. S5, demonstrates the clear distinction between a donor-derived $GFP^+AQP\text{-}5^+CD31^-$ or $GFP^+AQP\text{-}5^-CD31^+$ cells and a host-derived $GFP^-AQP\text{-}5^-$ $CD31^+$

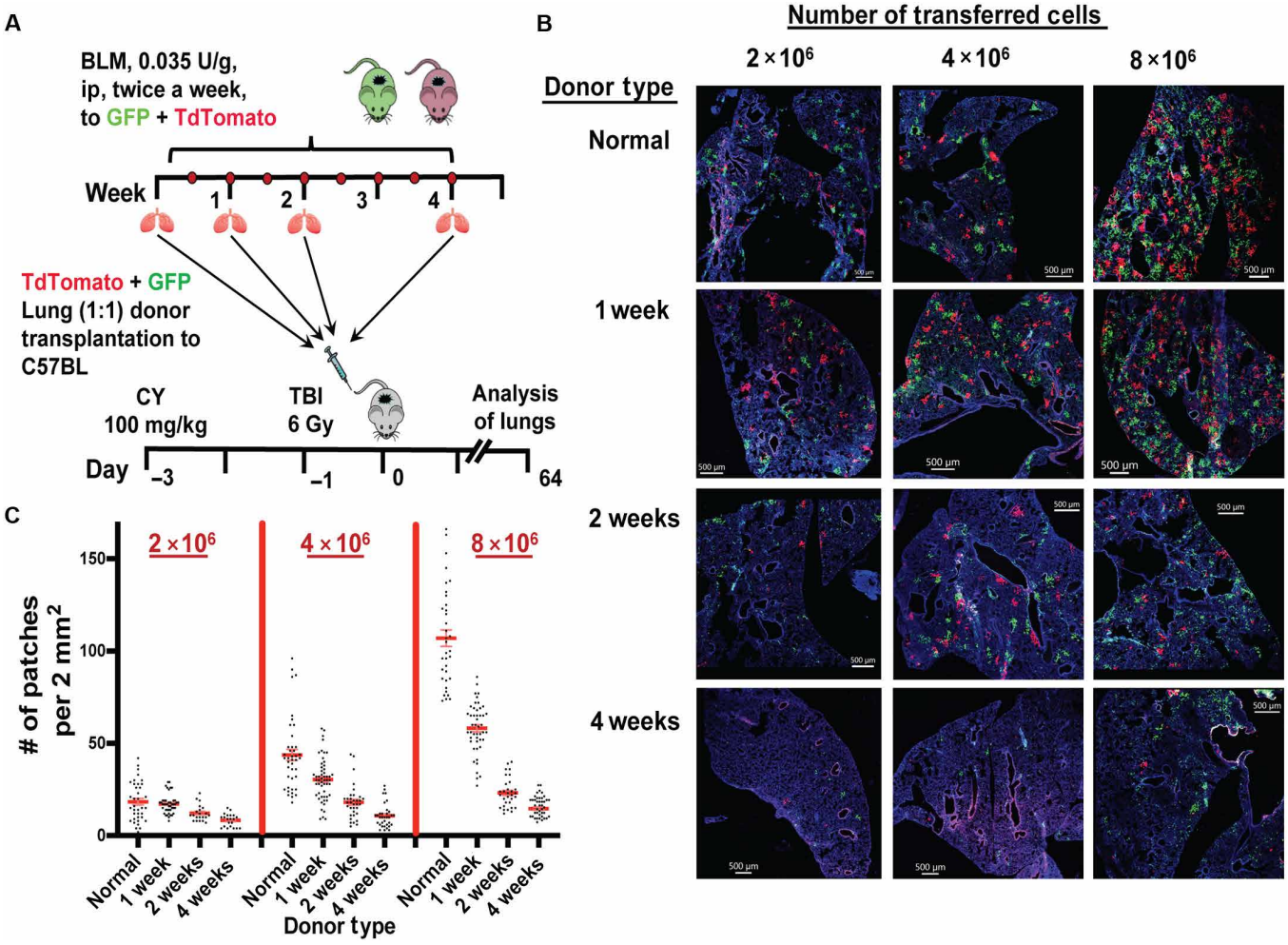

Fig. 2. Patch-forming lung progenitors in donor mice treated with BLM for different time periods. (**A**) TdTomato$^+$ and GFP$^+$ C57BL/6 male mice (donors) were treated with BLM for 1, 2, or 4 weeks, and thereafter, mice were euthanized, and a single-cell suspension derived from the lungs (1:1 mixture of both fluorescent donor types) was transplanted at different cell doses (2×10^6, 4×10^6, or 8×10^6 cells) into recipient mice conditioned with CY and 6-Gy TBI. Donor-derived patches were determined in the lungs of recipient mice at 64 days after transplantation. (**B**) Typical staining at 64 days after transplantation of donor-derived lung patches (TdTomato or GFP-positive) in lungs of mice receiving lung cells from donors treated with BLM for 1, 2, or 4 weeks. Scale bars, 500 µm. (**C**) Quantitative analysis of the number of donor-derived patches per 2-mm^2 lung area in the lungs of recipient mice at 64 days after transplantation (20 to 50 regions of 2 mm^2 were counted, from three to four mice in each group).

or GFP$^-$AQP-5$^+$ CD31$^-$ cells. Furthermore, as shown in fig. S7, donor-derived AT1, AT2, and endothelial cells are incorporated into alveoli and blood vessel structures. Quantitative analysis of the frequency of each cell type within the GFP$^+$ lung patches of chimeric mice is shown in Fig. 4 (column e). In this analysis, double staining of each cell type was ascertained by its consistency along 3 mm of the *z* axis. Typical examples of *z*-axis analysis for the different cell types are shown in fig. S6.

Together, this analysis revealed marked levels of donor-derived AT1, AT2, endothelial, and mesenchymal cells. As described above, and in line with extensive literature (*11*, *49*, *52*–*56*), the robust AT1 and AT2 lung chimerism could be of particular relevance for IPF therapy.

Therapeutic efficacy of lung cell transplantation in the BLM mouse model

The marked engraftment of donor-derived patch-forming lung progenitors attained upon transplantation at 1 week, after 4 weeks of BLM treatment (Fig. 5, A to C), was associated with reduced fibrosis compared to BLM-treated mice that did not receive a lung cell transplant (Fig. 5, D to G, and fig. S10A). Thus, the Ashcroft test measuring trichrome staining (Fig. 5, D and E), the hydroxyproline assay for collagen levels (Fig. 5F), α-SMA and HA staining (fig. S10A), and CT analysis (Fig. 5G) revealed lower levels of fibrosis in the transplanted compared to the non-transplanted group ($P < 0.002$ and $P < 0.0001$, respectively). Furthermore, the reduced level of fibrosis was also associated with improved lung function, measured by forced expired volume ($P < 0.0002$), commonly used to assess function in patients with IPF, as well as resistance ($P < 0.0002$), tissue damping ($P < 0.002$), and tissue elastance ($P < 0.002$) (Fig. 5H).

Successful engraftment of donor-derived progenitor cells in the *SPC-Cre TRF1$^{fl/fl}$* mouse model without conditioning treatment

Although the BLM mouse model is used extensively for testing new potential agents for the treatment of lung fibrosis, a model more

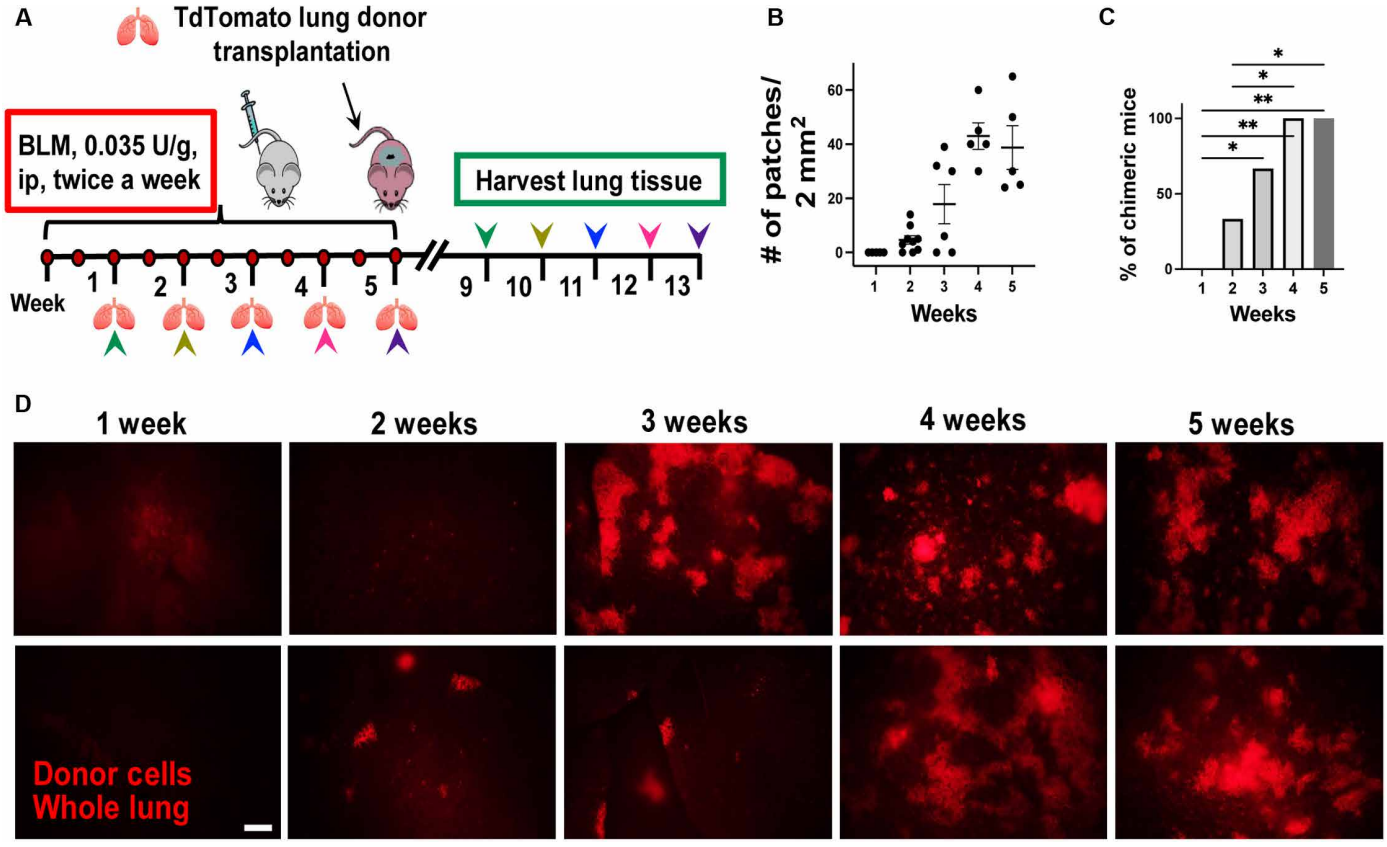

Fig. 3. Donor-derived patches after transplantation of TdTomato$^+$lung cells into recipient mice treated with BLM for different periods. (**A**) Experimental scheme. Recipient mice were treated with different numbers of BLM doses as indicated by the colored arrows. After completion of BLM treatment, the mice were transplanted with 8×10^6 TdTomato lung cells. The lungs were harvested and assessed for the level of donor-derived patches 8 weeks after transplantation. (**B**) Number of donor-derived lung patches per 2-mm^2 lung area in recipient mice treated with BLM for different periods. Each dot represents an average number of patches per 2 mm^2 based on at least 10 measurements in each individual mouse. Serial sections, 12 μm in thickness, were taken along the longitudinal axis of the lobe. A fixed distance (30 to 40 μm) between the sections was maintained to allow analysis at different depths of the lung, analyzing at least 10 sections across the entire lung. Lung slices were analyzed by fluorescence microscopy. (**C**) Percentage of chimeric mice, defined by at least four visible donor-derived patches consisting of more than 20 donor cells each. For groups analyzed after 1, 2, 3, 4, and 5 weeks of BLM treatment, $N = 5$, 9, 6, 5, and 5 mice, respectively. (**D**) Typical examples of donor-derived (red) lung patches in low magnification views of the lung of recipient mice treated with BLM for different periods. Scale bar, 500 μm. The top and bottom panels show separate examples of two representative mice from each group. *$P < 0.05$, **$P < 0.002$.

closely representing the IPF disease process was described recently (*37*, *56*). In this model, TRF1 is deleted specifically in AT2 cells upon treatment with TMX (Fig. 6, A and B), thereby inducing senescence in these cells, which, in turn, leads to progressive fibrosis, as shown by CT (Fig. 6, C and D). Thus, this model simulates more closely the fibrosis found in patients with IPF, in whom the disease is sometimes associated with defects in telomere maintenance (*11*, *49*).

As shown in Fig. 6 (E to G), the degree of chimerism induction after transplantation in the *SPC-Cre TRF1$^{fl/fl}$* model, similar to the BLM model, correlates with the progression of fibrosis. Lung cell transplantation at 2 or 4 weeks after completion of the TMX course (total of 8 to 10 weeks from the initiation of the experiment) did not lead to notable chimerism, while transplantation at 6 to 8 weeks after completion of TMX treatment (total of 12 to 14 weeks) resulted in marked levels of donor-derived patches without the need for any additional conditioning.

The time course of host progenitor ablation was shown by quantitative analysis of the number of donor-derived patches per 2-mm^2 lung area in the lungs of recipient mice (Fig. 6, F and G). Also, the different levels of chimerism following transplantation at different time points following completion of TMX treatment are illustrated per group by low power views of the lung (Fig. 6E). Additional eight examples of such views representing the variability of chimerism among 16 mice transplanted 7 weeks after completion of TMX treatment are shown in fig. S8.

Identification of donor-derived epithelial, endothelial, and mesenchymal cells in the *SPC-Cre TRF1$^{fl/fl}$* mouse model

To assess engrafted donor-derived patches obtained following transplantation at 14 weeks after initiation of TMX treatment, mice were transplanted with lung cells from C57BL/6-GFP$^+$ donors. As described for the BLM model, quantitative chimerism was assessed at 8 weeks after transplantation. Typical double staining of different donor-derived lung cell types is shown in Fig. 7 (A to D), and further verification of staining along 3 mm of the *z* axis was used to rule out potential errors in tracking the boundaries of each donor-derived cell (fig. S9).

To quantitate alveolar, endothelial, and mesenchymal cells, we used staining for GFP and different cell markers, as illustrated in

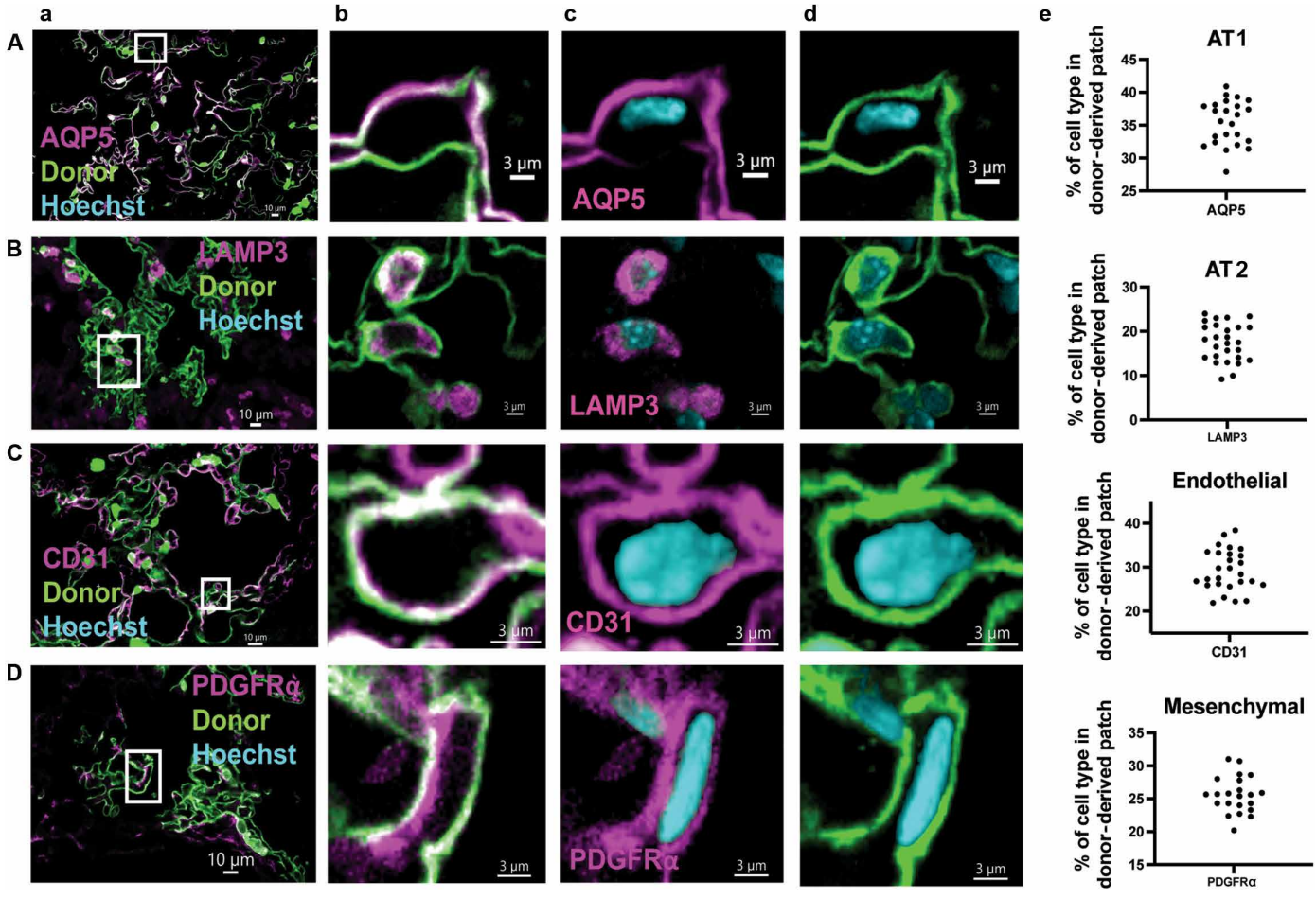

Fig. 4. Cell composition of GFP$^+$ donor-derived patches in the lungs of transplanted mice following treatment with BLM for 4 weeks. (**A** to **D**) Typical immunohistological staining of different lung cell types including (A) AQP5$^+$ AT1 alveolar cells, (B) LAMP3$^+$ AT2 alveolar cells, (C) CD31$^+$ endothelial cells, and (D) PDGFRα$^+$ mesenchymal cells. For each staining, low magnification (left column a; scale bars, 10 μm) shows a donor-derived GFP$^+$ patch (green), followed by high magnification of the indicated area within each patch (right columns b to d; scale bars, 3 μm) showing typical staining with different markers. Column b: Double staining GFP expression plus indicated marker (magenta). Column c: Indicated marker (magenta) plus nuclear staining (cyan). Column d: GFP (green) and nuclei (Hoechst, cyan). Column e: Distribution of average percentages of different cell types in donor-derived lung patches. To quantitate donor-derived AT1, AT2, endothelial, and mesenchymal cells, we used double staining for GFP with different cell markers, as illustrated in (A) to (D) or in figs. S5 and S6. To rule out potential errors in tracking the boundaries of each donor-derived cell in this quantitative analysis, verification of staining along 3 mm of the *z* axis (at 1-mm intervals) (as illustrated in fig. S6) was performed for every counted cell. Cells exhibiting staining that was not consistent across the *z* axis were not included in the final percentage analysis of donor-derived lung cell subpopulations. The figure represents a minimum of 20 patches for each staining obtained from three to six chimeric mice.

Fig. 7 (A to D) and fig. S9. In addition, verification of staining along 3 mm of the *z* axis (as illustrated in fig. S9) was performed for every counted cell in this quantitative analysis to rule out potential errors in tracking the boundaries of each donor-derived cell. Cells exhibiting staining that was not consistent across the *z* axis were not included in the final quantitation of the donor-derived lung cell subpopulations. The figure represents a minimum of 20 patches for each staining obtained from three to five chimeric mice.

Therapeutic efficacy of lung cell transplantation in the *SPC-Cre TRF1$^{fl/fl}$* mouse model

Last, transplanted *SPC-Cre TRF1$^{fl/fl}$* mice also exhibited an arrest in progression of lung fibrosis as indicated by the Ashcroft test (Fig. 8G), the hydroxyproline assay for collagen levels (Fig. 8H), α-SMA and HA staining (fig. S10B), and tests of lung function (Fig. 8I). These experiments further demonstrate the curative potential of intravenous administration of single-cell suspensions of lung tissue in the treatment of lung fibrosis.

DISCUSSION

Despite the emergence of innovative compounds for the treatment of patients with IPF, lung transplantation remains the only "curative" option, albeit with a low 5-year mean survival rate following transplantation. These poor outcomes highlight the urgent need for pioneering therapies. Our present study, investigating the efficacy of lung stem cell transplantation in two distinct models of lung fibrosis, clearly shows that lung cell transplantation is efficacious histologically, biochemically, radiographically, and physiologically. Our studies involved three independent transplantation experiments in

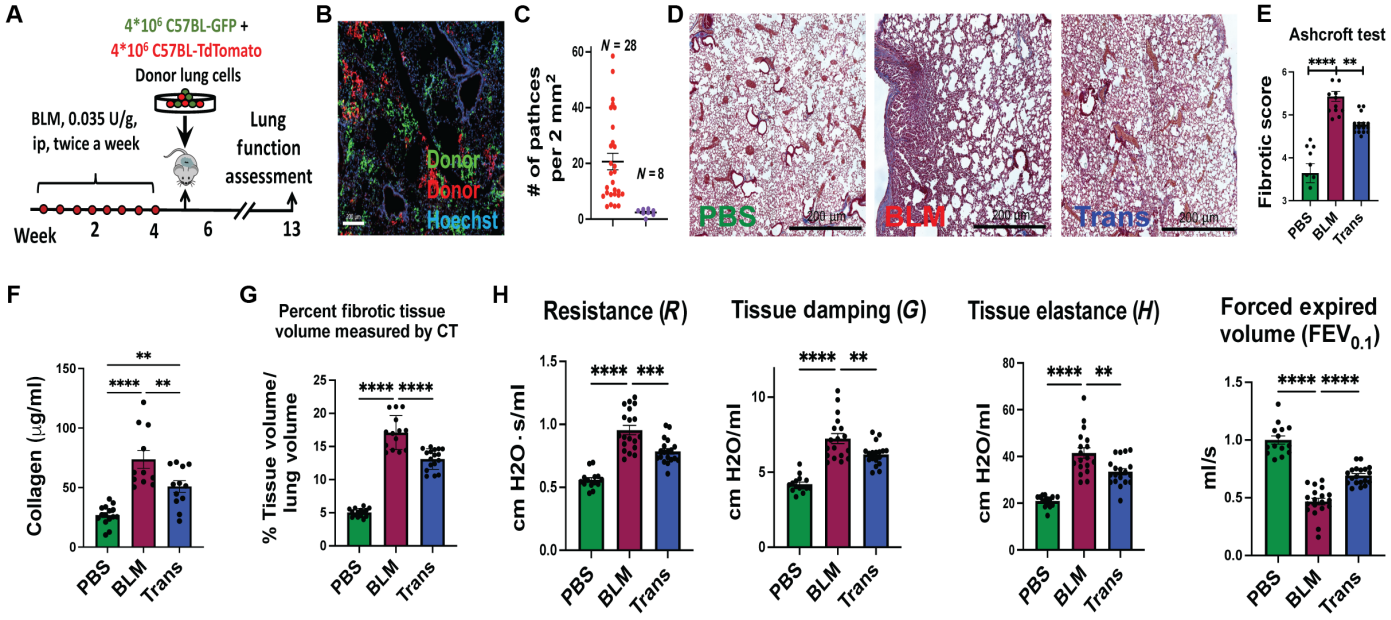

Fig. 5. Attenuation of fibrosis and functional benefit in the BLM mouse model 8 weeks after transplantation of lung cells. (**A**) Experimental scheme. Mice were treated with BLM and transplanted with 4×10^6 GFP$^+$ and 4×10^6 TdTomato$^+$ lung cells. (**B**) Fluorescence imaging of transplanted lung tissue 8 weeks after transplantation of a 1:1 mixture of TdTomato$^+$ and GFP$^+$ C57BL donor-derived lung cells. Scale bar, 200 µm. (**C**) Chimerism level defined by the average patch number per 2-mm^2 lung area. Mice exhibiting less than an average of four patches per 2-mm^2 lung tissue (purple) were excluded from further comparisons. Data were pooled from two independent experiments. (**D**) Trichrome staining of lung treated with vehicle (PBS), BLM, or BLM with transplantation of 8×10^6 donor-derived cells (Trans). Scale bars, 200 µm. All groups were examined for fibrosis 13 weeks after initiation of BLM treatment. (**E**) Ashcroft test comparing fibrosis levels based on trichrome staining. Mice were pooled from two independent transplantation experiments. For the PBS group, $N = 8$; for BLM alone, $N = 11$; and for BLM plus transplantation, $N = 15$ mice. (**F**) Quantitation of total collagen in the paraffin-embedded lung tissue by hydroxyproline assay, from one transplantation experiment. For PBS, $N = 14$; for BLM alone, $N = 11$; and for chimeric mice (Trans), $N = 12$. (**G**) Percent fibrotic lung tissue out of the total lung volume by CT. Results were pooled from two independent transplantation experiments. For PBS, $N = 15$; for BLM alone, $N = 15$; and for chimeric mice (Trans), $N = 17$. (**H**) Functional parameters measured by FlexiVent (one-way ANOVA with Dunnett's test; $^{**}P < 0.002$ and $^{****}P < 0.0001$). The lung function of mice was pooled from two independent transplantation experiments. For PBS, $N = 15$; BLM alone, $N = 19$; and for chimeric mice, $N = 19$.

each model, including at least two for functional analysis. Thus, we found in most transplanted mice that donor-derived patches occupy a substantial volume of the lungs, with more than 12 donor-derived patches per 2-mm^2 lung area, following transplantation of a lung cell suspension into mice exhibiting moderate levels of lung fibrosis. Immunohistochemical analysis showed that in both fibrosis models, the numerous donor-derived patches comprise AT1 (AQP5$^+$) and AT2 (LAMP3$^+$) alveolar cells, as well as endothelial (CD31$^+$) and mesenchymal (PDGFRα$^+$) cells. Furthermore, functional analysis measuring lung tissue resistance, elastance, and forced expired volume shows that this robust chimerism is associated with improved lung function in all parameters. Pathological analysis of the tissue also revealed a notable reduction in fibrotic tissue compared to non-transplanted mice.

Notably, the progression of lung fibrosis is associated with marked depletion of endogenous patch-forming lung progenitors in the recipients, thereby rendering them receptive to donor cell engraftment without any need for further conditioning. This unexpected finding further supports our earlier suggestion that, as in bone marrow transplantation (BMT), stem cell competition for lung stem cell niches represents a major barrier to attaining lung chimerism following lung stem cell transplantation. The lack of stem cell competition along the progression of fibrosis in our two mouse models is reminiscent of BMT in patients with severe combined immunodeficiency. These patients bear genetically defective T cell progenitors that are unable to compete with donor-derived normal progenitors, which can develop in the recipient's thymus following transplantation, without any need for host stem cell ablation (*57*, *58*). Thus, in the BLM model, the optimal time for engraftment was found at 3 to 4 weeks after initiation of BLM treatment (total of six to eight administrations of BLM), and in the *SPC-Cre TRF1$^{fl/fl}$* model, at 6 to 7 weeks following completion of knockout of TRF1 expression (total of 12 to 14 weeks from TMX treatment initiation). In contrast, only poor lung chimerism was observed in either model at earlier time points. Moreover, using CT analysis, we show that a level of fibrosis occupying about 15% or more of the lung is likely required for effective engraftment and colonization of the lung by donor-derived patch-forming lung progenitors (Fig. 6D). This level of fibrosis is similar to that found by CT in patients with IPF with moderate fibrosis (*59*, *60*). Such patients are likely to benefit from initiation of cellular therapy, and by that stage, the disease is on an invariably fatal trajectory.

Together, our results in two mouse models of pulmonary fibrosis offer a proof of concept for a simple and effective approach to lung repair. Notably, in patients with IPF, subclinical injury of the epithelium is associated with AT2 cell attrition and the presence of a subset of dysfunctional AT2 cells. Furthermore, AT2 cells in IPF exhibit a pro-fibrotic phenotype likely leading to the activation of fibroblasts, mesenchymal cell expansion, and ECM deposition. All these changes are associated with the failure of AT2 cells

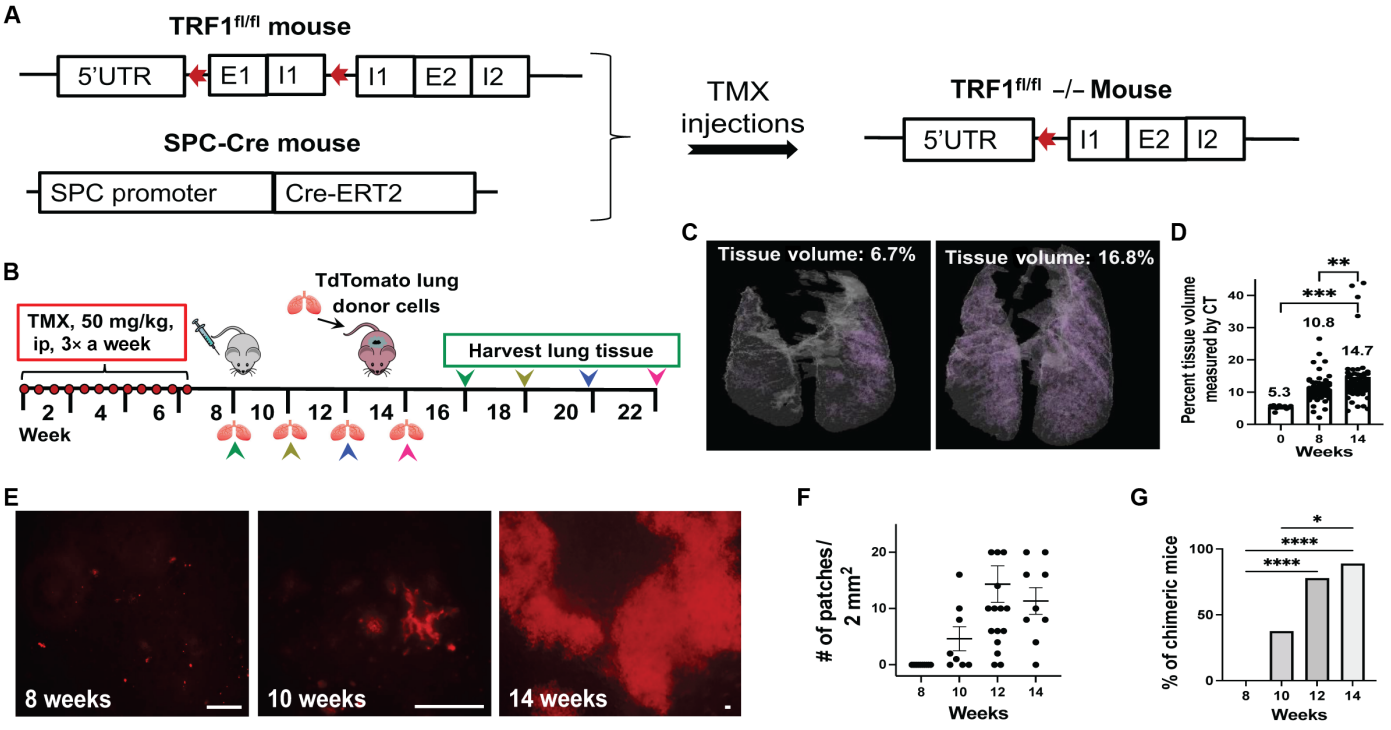

Fig. 6. Donor-derived patches after transplantation of TdTomato$^+$ lung cells into *SPC-Cre TRF1$^{fl/fl}$* mice at different time points after TMX treatment. (**A**) Generation of the *SPC-Cre TRF1$^{fl/fl}$* knockout (KO) mouse. TMX-induced Cre recombination leads to the deletion of TRF1 specifically in SPC$^+$ AT2 alveolar cells. E1 and E2, exons 1 and 2; I1 and I2, introns 1 and 2. Red arrows indicate Lox sequences. (**B**) Mice were then transplanted with lung cells from TdTomato$^+$ donors at the indicated time points (colored arrows) after TMX treatment and harvested 8 weeks after transplantation. (**C**) Representative 3D micro-CT imaging of normal lung tissue (left), and 14 weeks after initiation of TMX administration (right). Tissue volume (fibrotic area) is marked in purple. (**D**) Percent fibrosis (by micro-CT) at different time points after TMX without lung cell transplantation. Results were pooled from three independent experiments. Untreated mice, $N = 7$; 8 weeks from TMX initiation, $N = 20$; and 14 weeks from TMX initiation, $N = 30$. (**E**) Typical donor-derived (red) lung patches in whole-lung tissue of mice treated with donor lung cells at different time points after TMX initiation. Scale bars, 200 μm. (**F**) Number of donor-derived lung patches per 2-mm^2 lung area in transplanted mice at different time points after TMX induction. Each dot represents the average number of patches per 2 mm^2 based on at least 10 measurements in individual mice. Serial 12-μm sections, along the longitudinal axis of the lobe. Sections were taken every 30 to 40 μm for analysis at different lung depths. (**G**) Percentage of chimeric mice, with at least four visible donor-derived patches of more than 20 donor cells each. In (F) and (G), results were pooled from two independent transplantation experiments. For 8, 10, 12, and 14 weeks from initiation of TMX, $N = 7$, 8, 15 and 9 mice, respectively. One-way ANOVA with Dunnett's test; *$P < 0.05$, **$P < 0.002$, ***$P < 0.0002$, and ****$P < 0.0001$.

to differentiate into AT1 alveolar cells and the disruption of the epithelial-mesenchymal interface (*49*, *61*). It is increasingly believed that AT2 cell erosion leads to opportunistic expansion of fibroblasts, which further compromises the gas exchange properties of the lung surface (*61*, *62*).

Several preclinical studies suggesting the potential use of AT2 cell transplantation in the BLM fibrosis rat model have resulted in marked attenuation of the fibrogenic process (*63*, *64*). A phase 1/2 clinical trial indicated that allogenic AT2 lung cells can be administered safely via the trachea in patients with moderate progressive IPF under tacrolimus-based immune suppression (*64*). However, no evidence was presented for durable donor-derived lung chimerism, and further data regarding the clinical benefit of this cell therapy modality were not provided. Moreover, this approach requires repeated intratracheal infusions of AT2-enriched lung cell populations generated by prolonged ex vivo culture (*64*).

More recently, additional study in the field demonstrated progress in efforts aiming to generate lung progenitors from murine PSCs to form self-renewing lung epithelial progenitors able to engraft into the injured distal lung epithelium of immunocompetent, syngeneic mouse recipients (*32*). After transplantation, these progenitors mature in the distal lung, assuming the molecular phenotypes of AT2 and AT1 cells. These donor-derived cells retain their mature phenotypes, as characterized by scRNA-seq, histologic profiling, and functional assessment demonstrating the continued capacity of the engrafted cells to proliferate and differentiate. However, while showing a low but substantial level of chimerism in BLM-treated mice, there was no assessment of functional improvement following transplantation. Also, considering the transient nature of fibrosis in this mouse model, this approach should be further interrogated in long-term fibrosis models such as the TRF-SPC^{ko} model used in our study.

Another advancement in lung regeneration by cell therapy has been described very recently by Wang *et al.* (*65*) who performed an open-label clinical trial of ex vivo expanded autologous P63$^+$ lung progenitor cells for the treatment of patients with chronic obstructive pulmonary disease. Cells were collected during bronchoscopy, expanded over several weeks, and were then administered back into the patient's lungs, by repeat bronchoscopy. The treated group showed improvements in the diffusing capacity of the lung for carbon monoxide and in a 6-min walk distance at a 24-week follow-up. One advantage of this approach is in its use of syngeneic lung

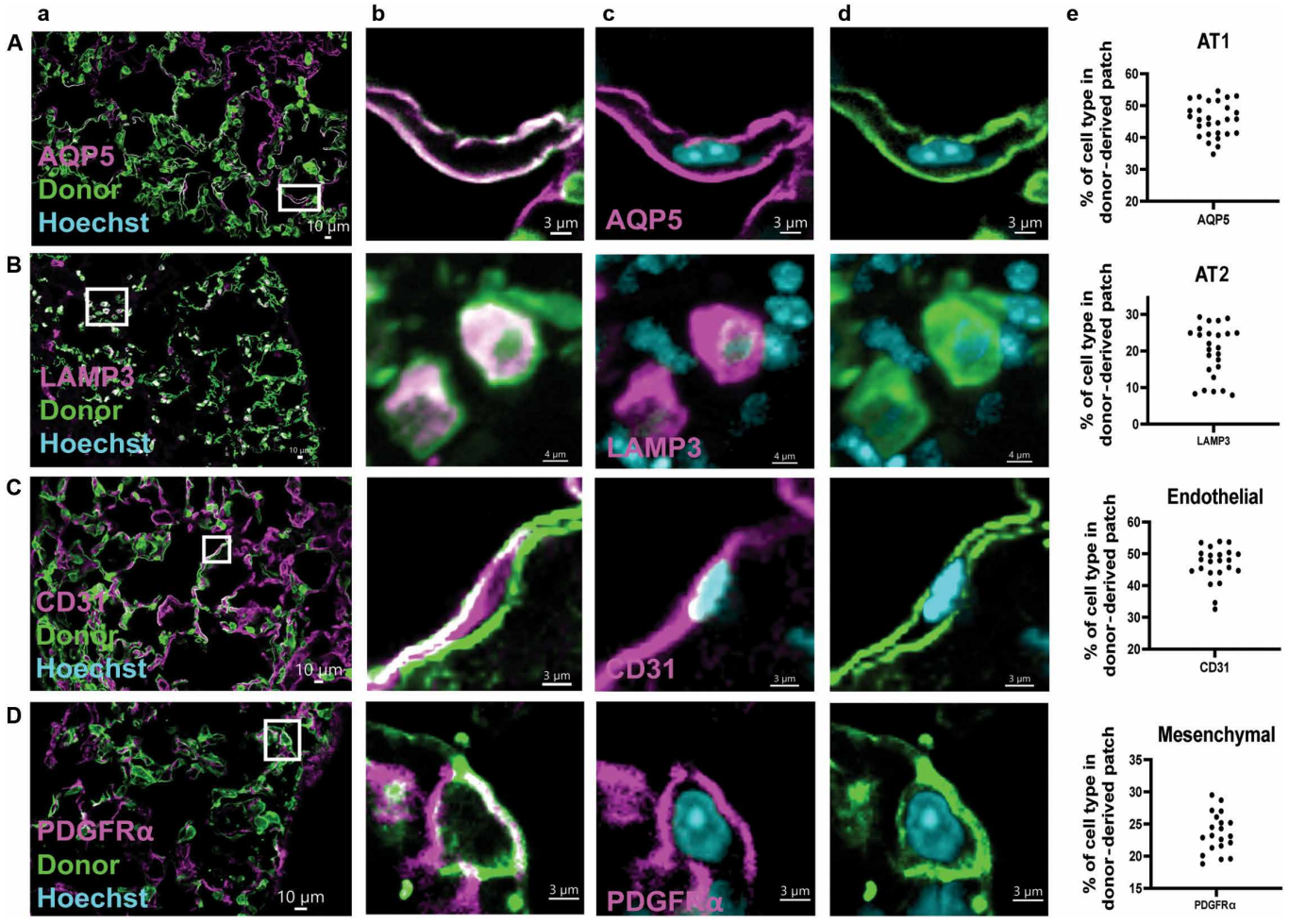

Fig. 7. Typical cell composition of C57BL/6-GFP$^+$ donor-derived patches in the lung of *SPC-Cre TRF1$^{fl/fl}$* mice transplanted 14 weeks after TMX treatment initiation and harvested 8 weeks after transplantation. (**A** to **D**) Typical immunohistological staining of different lung cell types including (A) AQP5$^+$ AT1 alveolar cells, (B) LAMP3$^+$ AT2 alveolar cells, (C) CD31$^+$ endothelial cells, and (D) PDGFRα$^+$ mesenchymal cells. For each staining, low magnification (left column a; scale bars, 10 µm) shows a donor-derived GFP$^+$ patch (green), followed by high magnification of the indicated area within each patch [right columns b to d; scale bars, 4 (B) and 3 µm (A, C, and D)] showing typical staining with different markers. Column b: Double staining GFP expression plus indicated marker (magenta). Column c: Indicated marker (magenta) plus nuclear staining (cyan). Column d: GFP (green) and nuclei (Hoechst, cyan). Column e: Distribution of average percentages of different cell types in donor-derived lung patches.

progenitors not requiring posttransplant immune suppression. However, further clinical trials are required to ascertain its full potential for clinical use. Notably, the major advantage of the transplant modality presented in the present study is in its simplicity using freshly isolated lung cells without any need for prolonged ex vivo expansion, which could potentially be associated with some risk for tumorigenicity and is also more difficult for extension to other medical centers.

Thus, our study demonstrates that infusion of a lung cell suspension can lead to robust regeneration of both donor-derived AT2 and AT1 alveolar cells, as well as endothelial cells. This multi-lineage engraftment could be particularly valuable and may offer a substantial advantage for lung function repair, considering that all major fibrotic diseases of the lung not only involve epithelial injuries but are also associated with vascular and endothelial damage, leading to poor oxygen exchange in the lungs. It should also be noted that while the robust regeneration of AT2 and AT1 alveolar cells is consistent with the prevention of fibrosis progression, the therapeutic impact in our mouse models was attained in the marked presence of donor-derived PDGFRα$^+$ mesenchymal progenitor cells. Further analysis of the potential individual contribution of donor-derived AT1 versus AT2, endothelial or mesenchymal progenitors cells, using donor mice expressing inducible diphtheria toxin under the lineage-specific promoter for each cell type, should shed light on the contribution of different donor-derived cell types to the attenuation of fibrosis progression in these models.

Together, our results strongly suggest that this transplantation modality could be successfully applied without any conditioning to patients exhibiting moderate fibrosis of the lungs, as documented by CT. In particular, our two distinct models suggest clinical potential for the treatment of lung fibrosis resulting from chemotherapy-induced lung injury or genetic susceptibility to progenitor depletion in IPF.

Considering that the application of this approach will potentially involve the use of allogeneic lung cells from major histocompatibility

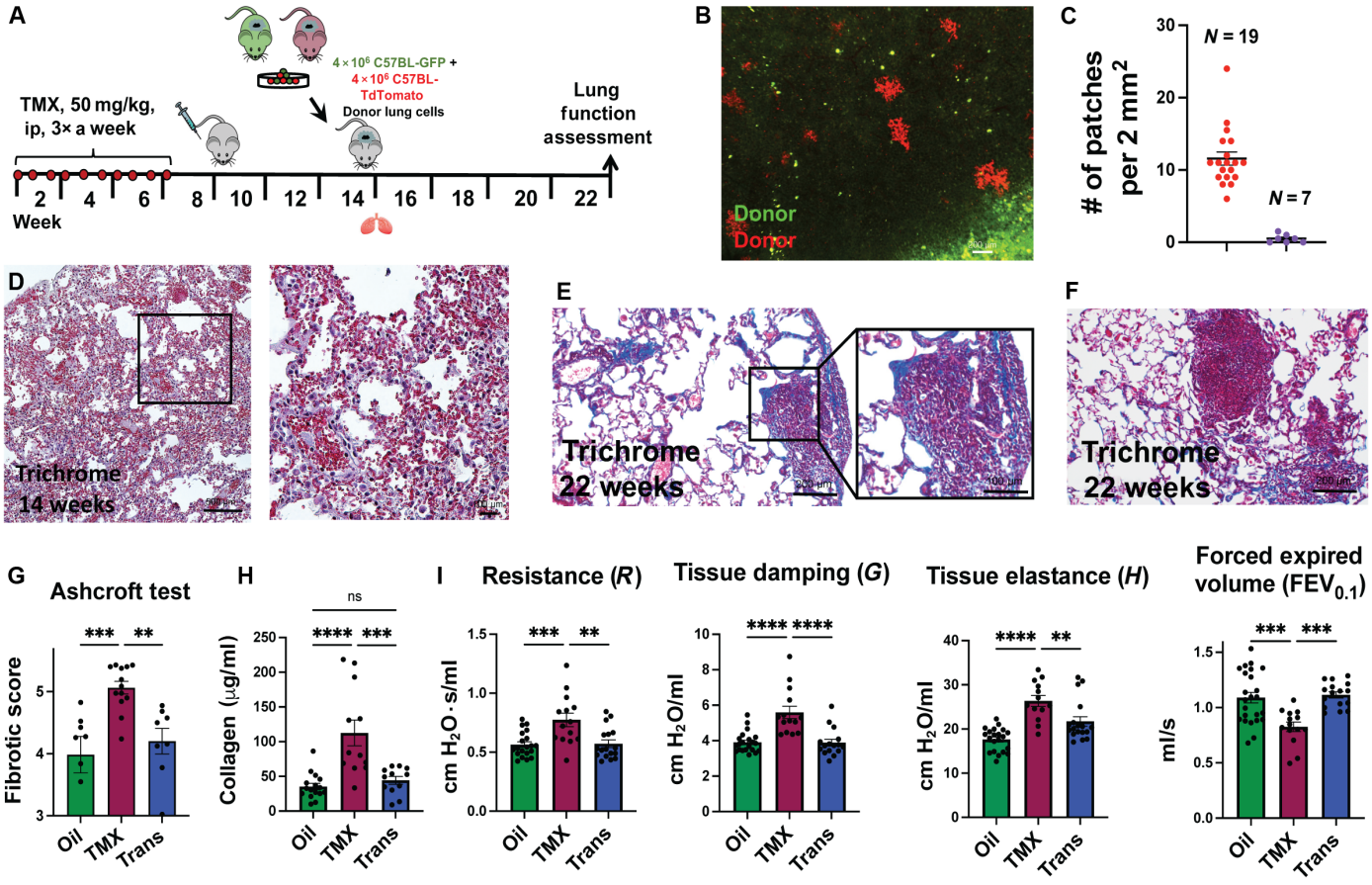

Fig. 8. Fibrosis attenuation and functional benefit in the *SPC-Cre TRF1$^{fl/fl}$* mouse model transplanted 14 weeks after initiation of TRF1 knockout. (**A**) Induction of TRF1 KO in AT2 cells by TMX treatment. Mice were transplanted with lung cells from C57BL/6-GFP$^+$ and TdTomato$^+$ donors 14 weeks after initiation of TMX treatment. (**B**) Fluorescence imaging of transplanted lung tissue 8 weeks after transplantation of a 1:1 mixture of TdTomato$^+$ and GFP$^+$ C57BL donor-derived lung cells following 14 weeks of host preconditioning. Scale bar, 200 μm. (**C**) Chimerism level defined by the average patch number per 2-mm^2 lung area. Mice exhibiting less than four patches per 2-mm^2 lung tissue (purple) on average were excluded from further comparisons. Results show that mouse data were pooled from two independent transplantation experiments. (**D**) Left: Typical fibrosis determined by trichrome staining 14 weeks after initiation of TMX induction. Right: Higher magnification of the area in the square (scale bars, 500 and 100 μm, respectively). (**E** and **F**) Two examples of fibrosis determined by trichrome staining 22 weeks after initiation of TMX induction (scale bars, 200 and 100 μm, respectively). (**G**) Ashcroft test comparing fibrosis levels in different groups of mice based on trichrome staining. Vehicle (oil)-treated group $N = 7$ mice; TMX alone, $N = 13$ mice; and TMX plus transplantation, $N = 7$ mice. (**H**) Quantitation of total collagen in the paraffin-embedded lung tissue, measured by the hydroxyproline assay. Data were pooled from two independent transplantation experiments; in the vehicle (oil)-treated group, $N = 13$ mice; in TMX alone, $N = 12$ mice; and for TMX plus transplantation, $N = 12$ mice. (**I**) Improved lung functional parameters measured by FlexiVent. Data in mice were pooled from two independent transplantation experiments. In the vehicle (oil)-treated group, $N = 21$ mice; in TMX alone, $N = 14$ mice; and in TMX plus transplantation, $N = 18$ mice. One-way ANOVA with Dunnett's test was used for statistical analysis; $^{**}P < 0.002$, $^{***}P < 0.0002$, and $^{****}P < 0.0001$.

complex disparate cadaveric donors, we expect that posttransplantation immune suppression, similar to that previously used safely in transplantation of AT2 cells (*64*), will be required. Clearly, T cells that are present in the donor lung suspension could induce harmful graft versus host disease; thus, the lung cell preparation protocol should include depletion of T cells by state-of-the-art methodologies commonly used in BMT.

While the major source for allogenic lung cell transplantation is currently limited to cadaveric lungs, it might be possible in the future to expand the patch-forming lung progenitors in culture, to enable harvesting of sufficient cells from lung biopsies of family members. Furthermore, as shown previously, induction of lung chimerism can be attained in mismatched recipients without any need for chronic immune suppression, by combining lung cell transplantation with BMT from the same donor (*35*, *66*). However, considering that the collection of sufficient numbers of hematopoietic stem cells from cadaveric lungs is difficult, this approach might be more feasible using live donors for the collection of ex vivo expanded lung progenitors, in conjunction with freshly isolated hematopoietic stem cells. In summary, our results provide a proof of concept for the use of intravenous infusion of lung cell suspensions for the treatment of lung fibrosis in patients with IPF and chemotherapy-induced lung injury.

MATERIALS AND METHODS

Experimental design

We previously showed that following adequate host conditioning with NA or CY, and sublethal 6-Gy TBI, transplanted lung progenitors

present in a single-cell lung suspension can integrate and engraft in the host lung tissue and can differentiate to epithelial (AT1 and AT2) and endothelial cells. In the present study, we evaluated the curative potential of intravenous lung cell transplantation in lung fibrosis. Thus, we successfully established and tested two mouse models of lung fibrosis, namely, the BLM and the TRF-SPC^{ko} (*SPC-Cre TRF1$^{fl/fl}$*) models. The impact of lung cell transplantation was evaluated in both models at 8 weeks after transplantation by lung function assay, CT imaging, and biochemical and histological analysis.

Mice

Animals were maintained under conditions approved by the Institutional Animal Care and Use Committee (IACUC) at MD Anderson Cancer Center (protocol nos. 1976 and 1819). Mouse strains used included the following: C57BL/6, C57BL/6-TRF1 (B6-129P2-Terf1$^{tm2.1Tdl}$), and B6-SPC-Cre [B6.129S-Sftpc$^{tm1(cre-ERT2)Blh}$], as well as donor mice for transplantation experiments including C57BL/6-Tg(CAG-EGFP)1Osb/J and B6.129(Cg)-*Gt(ROSA)26Sor$^{tm4(ACTB-tdTomato,-EGFP)Luo}$*/J. These latter mice express GFP or TdTomato, respectively, in all lung cells. All mice were used at 6 to 30 weeks of age. Mice were kept in small cages (up to five animals in each cage) and fed sterile food and water. Animals of the same age, sex, and genetic background were randomly assigned to treatment groups. Pre-established exclusion criteria were based on the IACUC guidelines and included systemic disease, respiratory distress, refusal to eat and drink, and substantial (>15%) weight loss. For BLM experiments, only male mice were used as hosts because male mice develop lung fibrosis to a greater degree than female mice (*67*). For experiments using the *SPC-Cre TRF1$^{fl/fl}$* model, mice of both genders were used as hosts. A minimum of five mice per group were used in all experiments.

Generation of the *SPC-Cre TRF1$^{fl/fl}$* genetic model

C57BL/6-TRF1 (B6-129P2-Terf1$^{tm2.1Tdl}$) were received from JAX Labs after cryo-recovery and backcrossed in our laboratory with C57BL/6 for four generations to ensure a clean C57BL/6 background. Mice homozygous for the Lox insertion were mated with transgenic mice that express Cre-ERT protein under the control of the lung surfactant promoter (SFTPC)-B6-SPC-Cre [B6.129S-Sftpc$^{tm1(cre-ERT2)Blh}$]. The first generation of heterozygous B6-TRF$^{WT/Lox}$ SPC-Cre-ERT mice was backcrossed within the group until we attained a strain of B6-SPC-Cre-ERT *TRF1$^{fl/fl}$* mice. To activate the Cre protein, mice were injected intraperitoneally with 50 mg of TMX per kilogram (Sigma-Aldrich) for 6 to 7 weeks, three injections per week. TMX was freshly dissolved in corn oil to a concentration of 10 μg/μl before each administration.

Induction of fibrosis by bleomycin

C57BL/6 male mice (*67*) aged 9 to 10 weeks were administered BLM (0.035 U/g; Hikma or Teva) by intraperitoneal injection twice a week for 1 to 5 weeks. Control groups were administered phosphate-buffered saline (PBS) vehicle. Mice were weighed twice a week, and those who lost weight were fed with extra high-fat food. Weight loss of more than 20% led to euthanizing the mice.

Preconditioning of host C57BL/6 mice before transplantation

To test the level of patch-forming lung progenitors after BLM treatment, we used an assay that we previously described (*35*) based on the conditioning of recipient mice with CY and 6-Gy TBI. On day −3 before transplantation, the C57BL/6 host mice were treated with an intraperitoneal injection of CY (200 mg/kg; Sandoz or Baxter) dissolved in PBS. On day −1 before transplantation, the mice were treated with 6-Gy TBI in an XRad320 biological x-ray irradiator. On day 0, the mice were transplanted with various cell populations, as indicated in Fig. 2.

Preparation of single-cell lung suspension

Single-cell suspensions were obtained from enzymatically treated adult mouse lungs, as previously described (*34*, *35*). Briefly, lung tissue was dissociated by mincing tissues with fine scissors in the presence of collagenase (1 mg/ml), dispase (2.4 U/ml), and deoxyribonuclease I (1 mg/ml) (Roche Diagnostics) diluted in $Ca^{+}Mg^{+}$ PBS. Cells were dissociated by GentalMax (Miltenyi Biotec) incubation for 30 min at 37°C. Nonspecific debris was removed by sequential filtration through 100- and 70-μm filters. The cells were then washed with PBS (Ca^{+2} and Mg^{+2} free) with 2% bovine serum albumin, antibiotics, and 2 mM anticoagulant citrate dextrose solution A. Before intravenous injection, the donor cells were filtered again through a 40-μm filter. Host mice were transplanted with 2×10^6 to 8×10^6 adult lung cells, labeled with either B6-GFP^{+} or B6-TdTomato^{+}. Transplanted cells were introduced by intravenous cell injection (intravenous) into the tail vein.

Flow cytometry

Cell samples were stained with conjugated antibodies or matching isotype controls according to the antibody manufacturer's instructions. Antibodies were purchased from e-Bioscience and BioLegend. The complete list of antibodies used in the study is provided in table S1. Data were acquired on BD FACSCanto II or BD LSRFortessa flow cytometer and analyzed using the FlowJo software (version 9 or version 10).

Immunostaining

Mice were euthanized at different time points following transplantation; the lungs were inflated with a 4% paraformaldehyde (PFA) solution introduced through the trachea under a constant pressure of 20 cm H_2O. Then, the lungs were immersed in fixative overnight at 4°C. The next day, the lungs were split into two halves—the first half was preserved in 30% sucrose for an additional 24 hours before snap-freezing in isopentane precooled by liquid nitrogen in the presence of optimal cutting temperature (OCT) compound (Sakura Finetek USA Inc., Tissue-Tek., product code #4583). The second half was preserved with 70% ethanol before paraffin embedding. The samples for frozen sections were harvested and inflated with a 1:1 mixture of OCT and PBS and snap-frozen in isopentane precooled by liquid nitrogen. Frozen samples were cut into 6- to 12-μm sections and stained. The list of antibodies used in this study is provided in table S1. All secondary antibodies were purchased from Jackson Laboratories or Abcam. The evaluation of stained samples was performed using an upright Olympus BX51 fluorescent microscope with 4×, 10×, and 20× air and 40× and 100× oil objectives and an Olympus digital camera (DP70). Confocal microscopy was performed on an Olympus 3000FV laser scanning confocal microscope, using cell sense software (Olympus). The images were processed, rendered, and reconstructed in 3D in Imaris software (Bitplane AG, Switzerland, www.bitplane.com).

Trichrome staining and Ashcroft test for fibrosis assessment

The lower-mid part of the right lungs, which were fixed by PFA, was deparaffinized and stained with Masson's trichrome using Masson Trichrome Staining Kit (Thomas Scientific) according to the manufacturer's instructions. More than 20 bright-field images per mouse were taken, using 20-fold magnification. The fields were chosen randomly by moving the stage controls of the microscope blindly and photographing the resulting field without further stage adjustments. The image files were coded and given to three different observers, blinded to the experimental groups. The observers were provided with a copy of the scoring scheme and a set of different grade examples. Each observer scored all the images from 0 to 8 using the specific criteria described in the paper by Ashcroft *et al.* (*68*) and Hubner *et al.* (*10*). All scores were then pooled, and the average was calculated per field and per mouse, and then per group with different treatments. The results were also divided into three scoring bins: A score of 0 to 3 represents normal lung tissue; a score of 4 to 5 indicates mild damage; and a score of 6 to 8 represents severe fibrotic damage. Results were analyzed using the PRISM software. Large field images were taken using ImageXpress Micro Confocal.

CT scan and calculation of fibrotic area

In vivo micro-CT scans were performed by high-resolution SKYSCAN 1276 (Bruker BioSpin Corporation, MA) at 30-μm resolution, 135-ms exposure time, 0.5-mm filter, and with the use of a 1008 × 672 matrix. Mice were anesthetized with 0.5% oxygen and 1.5% isoflurane. 3D images and fibrosis percentage calculations were performed using a 55/255 threshold. Lung volume (LV) and fibrosis volume (FV) were measured. The percent fibrosis (FV/LV) was calculated as the percent of FV out of total LV (*69*).

Quantitative assay for total collagen levels

To evaluate total collagen levels, we used an assay based on a colorimetric readout for free hydroxyproline (*70*). Briefly, paraffin-embedded lung samples were weighed and hydrolyzed overnight and then assessed by the color reaction for the amount of collagen using the QuickZyme kit (QuickZyme, Biosciences, Netherlands) according to the manufacturer's instructions.

Assessment of lung function

Respiratory system mechanics and P-V relationships were measured using the FlexiVent apparatus (SCIREQ, Montreal, QC, Canada), as previously described (*36*, *71*, *72*). Briefly, mice were anesthetized using Avertin, tracheotomized using a 19-gauge metal cannula (Brico), connected to the FlexiVent via endotracheal cannula, and ventilated at a respiratory rate of 150 breaths/min and tidal volume of 10 ml/kg against a positive end-expiratory pressure of 3 cm H_2O. FlexiVent software was used to perform the forced measurements and P-V loops.

The linear single-frequency forced oscillation technique (FOT) was used to assess total respiratory system resistance I, compliance I, and elastance I. The broadband FOT was used to determine Newtonian resistance (R_n), tissue elastance (H), and tissue dampening (G). Volume-driven P-V loops were formed by incrementally inflating the lungs to 40 ml/kg from functional residual capacity, which was defined as 3 cm H_2O. After the delivery of each volume increment, the airway opening pressure was recorded. The area of the P-V curve was calculated using FlexiVent software to provide data for quantitative analysis of the elastic properties. All measurements of respiratory system mechanics were conducted in mice with intact chest walls. Upon completion of the measurements, anesthetized animals were euthanized by cervical dislocation. Results were analyzed using the PRISM software.

Statistical analysis

Differences between groups were evaluated using one-way variance analysis (ANOVA) and Dunnett's post hoc test for calculating the P value between three or more different groups, or unpaired t test for comparison of two groups only, using the Prism software. For each dataset, means ± SD or means ± SEM was calculated and is presented in the Results section of the main text. $P \leq 0.05$ was considered statistically significant.

Supplementary Materials

This PDF file includes:

Supplementary Methods
Figs. S1 to S10
Table S1
References

REFERENCES AND NOTES

1. N. Jeganathan, M. Sathananthan, The prevalence and burden of interstitial lung diseases in the USA. *ERJ Open Res.* **8**, 10.1183/23120541.00630-2021 (2022).
2. World Health Organization, www.who.int/health-topics/chronic-respiratory-diseases#tab=tab_3.
3. E. P. Dove, A. L. Olson, M. K. Glassberg, Trends in idiopathic pulmonary fibrosis-related mortality in the United States: 2000-2017. *Am. J. Respir. Crit. Care Med.* **200**, 929–931 (2019).
4. Q. Zheng, I. A. Cox, J. A. Campbell, Q. Xia, P. Otahal, B. de Graaff, T. J. Corte, A. K. Y. Teoh, E. H. Walters, A. J. Palmer, Mortality and survival in idiopathic pulmonary fibrosis: A systematic review and meta-analysis. *ERJ Open Res.* **8**, 10.1183/23120541.00591-2021 (2022).
5. B. Langford, A. Diamantopoulos, T. M. Maher, Y. Inoue, K. B. Rohr, M. Baldwin, Using data on survival with idiopathic pulmonary fibrosis to estimate survival with other types of progressive fibrosis interstitial lung disease: A Bayesian framework. *Adv. Ther.* **39**, 1045–1054 (2022).
6. P. Janowiak, A. Szymanowska-Narloch, A. Sieminska, IPF respiratory symptoms management—Current evidence. *Front. Med.* **9**, 10.3389/fmed.2022.917973 (2022).
7. H. Fujimoto, T. Kobayashi, A. Azuma, Idiopathic pulmonary fibrosis: Treatment and prognosis. *Clin. Med. Insights Circ. Respir. Pulm. Med.* **9**, 179–185 (2015).
8. T. J. Gross, G. W. Hunninghake, Idiopathic pulmonary fibrosis. *N. Engl. J. Med.* **345**, 517–525 (2001).
9. K. Ask, R. Labiris, L. Farkas, A. Moeller, A. Froese, T. Farncombe, G. B. McClelland, M. Inman, J. Gauldie, M. R. Kolb, Comparison between conventional and "clinical" assessment of experimental lung fibrosis. *J. Transl. Med.* **6**, 16 (2008).
10. R. H. Hubner, W. Gitter, N. E. El Mokhtari, M. Mathiak, M. Both, H. Bolte, S. Freitag-Wolf, B. Bewig, Standardized quantification of pulmonary fibrosis in histological samples. *Biotechniques* **44**, 507–517 (2008).
11. F. J. Martinez, H. R. Collard, A. Pardo, G. Raghu, L. Richeldi, M. Selman, J. J. Swigris, H. Taniguchi, A. U. Wells, Idiopathic pulmonary fibrosis. *Nat. Rev. Dis. Primers.* **3**, 17074 (2017).
12. M. Selman, A. Pardo, L. Barrera, A. Estrada, S. R. Watson, K. Wilson, N. Aziz, N. Kaminski, A. Zlotnik, Gene expression profiles distinguish idiopathic pulmonary fibrosis from hypersensitivity pneumonitis. *Am. J. Respir. Crit. Care Med.* **173**, 188–198 (2006).
13. W. D. Travis, U. Costabel, D. M. Hansell, T. E. King Jr., D. A. Lynch, A. G. Nicholson, C. J. Ryerson, J. H. Ryu, M. Selman, A. U. Wells, J. Behr, D. Bouros, K. K. Brown, T. V. Colby, H. R. Collard, C. R. Cordeiro, V. Cottin, B. Crestani, M. Drent, R. F. Dudden, J. Egan, K. Flaherty, C. Hogaboam, Y. Inoue, T. Johkoh, D. S. Kim, M. Kitaichi, J. Loyd, F. J. Martinez, J. Myers, S. Protzko, G. Raghu, L. Richeldi, N. Sverzellati, J. Swigris, D. Valeyre; ATS/ERS Committee on Idiopathic Interstitial Pneumonias, An official American Thoracic Society/European Respiratory Society statement: Update of the international multidisciplinary classification of the idiopathic interstitial pneumonias. *Am. J. Respir. Crit. Care Med.* **188**, 733–748 (2013).
14. G. W. Hunninghake, M. B. Zimmerman, D. A. Schwartz, T. E. King Jr., J. Lynch, R. Hegele, J. Waldron, T. Colby, N. Muller, D. Lynch, J. Galvin, B. Gross, J. Hogg, G. Toews, R. Helmers, J. A. Cooper Jr., R. Baughman, C. Strange, M. Millard, Utility of a lung biopsy for the

diagnosis of idiopathic pulmonary fibrosis. *Am. J. Respir. Crit. Care Med.* **164**, 193–196 (2001).
15. J. P. Finnerty, A. Ponnuswamy, P. Dutta, A. Abdelaziz, H. Kamil, Efficacy of antifibrotic drugs, nintedanib and pirfenidone, in treatment of progressive pulmonary fibrosis in both idiopathic pulmonary fibrosis (IPF) and non-IPF: A systematic review and meta-analysis. *BMC Pulm. Med.* **21**, 411 (2021).
16. G. H. Hughes, H. Toellner, H. Morris, C. Leonard, N. Chaudhuri, Real world experiences: Pirfenidone and nintedanib are effective and well tolerated treatments for idiopathic pulmonary fibrosis. *J. Clin. Med.* **5**, 78 (2016).
17. P. Marijic, L. Schwarzkopf, L. Schwettmann, T. Ruhnke, F. Trudzinski, M. Kreuter, Pirfenidone vs. nintedanib in patients with idiopathic pulmonary fibrosis: A retrospective cohort study. *Respir. Res.* **22**, 268 (2021).
18. P. Rogliani, L. Calzetta, F. Cavalli, M. G. Matera, M. Cazzola, Pirfenidone, nintedanib and N-acetylcysteine for the treatment of idiopathic pulmonary fibrosis: A systematic review and meta-analysis. *Pulm. Pharmacol. Ther.* **40**, 95–103 (2016).
19. F. Varone, G. Sgalla, B. Iovene, T. Bruni, L. Richeldi, Nintedanib for the treatment of idiopathic pulmonary fibrosis. *Expert Opin. Pharmacother.* **19**, 167–175 (2018).
20. P. Rivera-Ortega, C. Hayton, J. Blaikley, C. Leonard, N. Chaudhuri, Nintedanib in the management of idiopathic pulmonary fibrosis: Clinical trial evidence and real-world experience. *Ther. Adv. Respir. Dis.* **12**, 10.1177/1753466618800618 (2018).
21. T. Moua, J. H. Ryu, Obstacles to early treatment of idiopathic pulmonary fibrosis: Current perspectives. *Ther. Clin. Risk Manag.* **15**, 73–81 (2019).
22. A. Tzouvelekis, J. D. Herazo-Maya, M. Slade, J. H. Chu, G. Deiuliis, C. Ryu, Q. Li, K. Sakamoto, G. Ibarra, H. Pan, M. Gulati, D. Antin-Ozerkis, E. L. Herzog, N. Kaminski, Validation of the prognostic value of MMP-7 in idiopathic pulmonary fibrosis. *Respirology* **22**, 486–493 (2017).
23. P. M. George, C. M. Patterson, A. K. Reed, M. Thillai, Lung transplantation for idiopathic pulmonary fibrosis. *Lancet Respir. Med.* **7**, 271–282 (2019).
24. A. P. Wong, A. E. Dutly, A. Sacher, H. Lee, D. M. Hwang, M. Liu, S. Keshavjee, J. Hu, T. K. Waddell, Targeted cell replacement with bone marrow cells for airway epithelial regeneration. *Am. J. Physiol. Lung Cell. Mol. Physiol.* **293**, L740–L752 (2007).
25. A. P. Wong, A. Keating, W. Y. Lu, P. Duchesneau, X. Wang, A. Sacher, J. Hu, T. K. Waddell, Identification of a bone marrow-derived epithelial-like population capable of repopulating injured mouse airway epithelium. *J. Clin. Invest.* **119**, 336–348 (2009).
26. P. Duchesneau, A. P. Wong, T. K. Waddell, Optimization of targeted cell replacement therapy: A new approach for lung disease. *Mol. Ther.* **18**, 1830–1836 (2010).
27. M. L. Bustos, M. Mura, P. Marcus, D. Hwang, O. Ludkovski, A. P. Wong, T. K. Waddell, Bone marrow cells expressing clara cell secretory protein increase epithelial repair after ablation of pulmonary clara cells. *Mol. Ther.* **21**, 1251–1258 (2013).
28. A. E. Vaughan, A. N. Brumwell, Y. Xi, J. E. Gotts, D. G. Brownfield, B. Treutlein, K. Tan, V. Tan, F. C. Liu, M. R. Looney, M. A. Matthay, J. R. Rock, H. A. Chapman, Lineage-negative progenitors mobilize to regenerate lung epithelium after major injury. *Nature* **517**, 621–625 (2015).
29. W. Zuo, T. Zhang, D. Z. Wu, S. P. Guan, A. A. Liew, Y. Yamamoto, X. Wang, S. J. Lim, M. Vincent, M. Lessard, C. P. Crum, W. Xian, F. McKeon, p63^{+}Krt5^{+} distal airway stem cells are essential for lung regeneration. *Nature* **517**, 616–620 (2015).
30. M. Nichane, A. Javed, V. Sivakamasundari, M. Ganesan, L. T. Ang, P. Kraus, T. Lufkin, K. M. Loh, B. Lim, Isolation and 3D expansion of multipotent Sox9^{+} mouse lung progenitors. *Nat. Methods* **14**, 1205–1212 (2017).
31. Q. Ma, Y. Ma, X. Dai, T. Ren, Y. Fu, W. Liu, Y. Han, Y. Wu, Y. Cheng, T. Zhang, W. Zuo, Regeneration of functional alveoli by adult human SOX9^{+} airway basal cell transplantation. *Protein Cell* **9**, 267–282 (2018).
32. M. J. Herriges, M. Yampolskaya, B. R. Thapa, J. Lindstrom-Vautrin, F. Wang, J. Huang, C. L. Na, L. Ma, M. M. Montminy, P. Bawa, C. Villacorta-Martin, P. Mehta, D. N. Kotton, Durable alveolar engraftment of PSC-derived lung epithelial cells into immunocompetent mice. *Cell Stem Cell* **30**, 1217–1234.e7 (2023).
33. C. Rosen, E. Shezen, A. Aronovich, Y. Z. Klionsky, Y. Yaakov, M. Assayag, I. E. Biton, O. Tal, G. Shakhar, H. Ben-Hur, D. Shneider, Z. Vaknin, O. Sadan, S. Evron, E. Freud, D. Shoseyov, M. Wilschanski, N. Berkman, W. E. Fibbe, D. Hagin, C. Hillel-Karniel, I. M. Krentsis, E. Bachar-Lustig, Y. Reisner, Preconditioning allows engraftment of mouse and human embryonic lung cells, enabling lung repair in mice. *Nat. Med.* **21**, 869–879 (2015).
34. I. Milman Krentsis, C. Rosen, E. Shezen, A. Aronovich, B. Nathanson, E. Bachar-Lustig, N. Berkman, M. Assayag, G. Shakhar, T. Feferman, R. Orgad, Y. Reisner, Lung injury repair by transplantation of adult lung cells following preconditioning of recipient mice. *Stem Cells Transl. Med.* **7**, 68–77 (2018).
35. I. Milman Krentsis, R. Orgad, Y. Zheng, E. Bachar Lustig, C. Rosen, E. Shezen, S. Yadav, B. Nathansohn Levi, M. Assayag, N. Berkman, H. Karmouty Quintana, E. Shoshan, C. Blagdon, Y. Reisner, Lung regeneration by transplantation of allogeneic lung progenitors using a safer conditioning regimen and clinical-grade reagents. *Stem Cells Transl. Med.* **11**, 178–188 (2022).
36. L. Headley, W. Bi, C. Wilson, S. D. Collum, M. Chavez, T. Darwiche, T. C. J. Mertens, A. M. Hernandez, S. R. Siddiqui, S. Rosenbaum, R. A. Johnston, H. Karmouty-Quintana, Low-dose administration of bleomycin leads to early alterations in lung mechanics. *Exp. Physiol.* **103**, 1692–1703 (2018).
37. J. M. Povedano, P. Martinez, J. M. Flores, F. Mulero, M. A. Blasco, Mice with pulmonary fibrosis driven by telomere dysfunction. *Cell Rep.* **12**, 286–299 (2015).
38. D. J. Schrier, R. G. Kunkel, S. H. Phan, The role of strain variation in murine bleomycin-induced pulmonary fibrosis. *Am. Rev. Respir. Dis.* **127**, 63–66 (1983).
39. I. I. Singer, D. W. Kawka, S. M. McNally, G. J. Eiermann, J. M. Metzger, L. B. Peterson, Extensive laminin and basement membrane accumulation occurs at the onset of bleomycin-induced rodent pulmonary fibrosis. *Am. J. Pathol.* **125**, 258–268 (1986).
40. A. Moeller, K. Ask, D. Warburton, J. Gauldie, M. Kolb, The bleomycin animal model: A useful tool to investigate treatment options for idiopathic pulmonary fibrosis? *Int. J. Biochem. Cell Biol.* **40**, 362–382 (2008).
41. Y. Aono, J. G. Ledford, S. Mukherjee, H. Ogawa, Y. Nishioka, S. Sone, M. F. Beers, P. W. Noble, J. R. Wright, Surfactant protein-D regulates effector cell function and fibrotic lung remodeling in response to bleomycin injury. *Am. J. Respir. Crit. Care Med.* **185**, 525–536 (2012).
42. J. Tashiro, S. J. Elliot, D. J. Gerth, X. Xia, S. Pereira-Simon, R. Choi, P. Catanuto, S. Shahzeidi, R. L. Toonkel, R. H. Shah, F. El Salem, M. K. Glassberg, Therapeutic benefits of young, but not old, adipose-derived mesenchymal stem cells in a chronic mouse model of bleomycin-induced pulmonary fibrosis. *Transl. Res.* **166**, 554–567 (2015).
43. F. Ruscitti, F. Ravanetti, J. Essers, Y. Ridwan, S. Belenkov, W. Vos, F. Ferreira, A. KleinJan, P. van Heijningen, C. Van Holsbeke, A. Cacchioli, G. Villetti, F. F. Stellari, Longitudinal assessment of bleomycin-induced lung fibrosis by Micro-CT correlates with histological evaluation in mice. *Multidiscip. Respir. Med.* **12**, 8 (2017).
44. M. A. Mouratis, V. Aidinis, Modeling pulmonary fibrosis with bleomycin. *Curr. Opin. Pulm. Med.* **17**, 355–361 (2011).
45. D. M. Walters, S. R. Kleeberger, Mouse models of bleomycin-induced pulmonary fibrosis. *Curr. Protoc. Pharmacol.* **40**, 5.46.1–5.46.17 (2008).
46. I. Y. Adamson, D. H. Bowden, The pathogenesis of bleomycin-induced pulmonary fibrosis in mice. *Am. J. Pathol.* **77**, 185–197 (1974).
47. T. Yanagihara, S. G. Chong, M. Vierhout, J. A. Hirota, K. Ask, M. Kolb, Current models of pulmonary fibrosis for future drug discovery efforts. *Expert Opin. Drug Discovery* **15**, 931–941 (2020).
48. G. Izbicki, M. J. Segel, T. G. Christensen, M. W. Conner, R. Breuer, Time course of bleomycin-induced lung fibrosis. *Int. J. Exp. Pathol.* **83**, 111–119 (2002).
49. Z. Borok, J. A. Whitsett, P. B. Bitterman, V. J. Thannickal, D. N. Kotton, S. D. Reynolds, M. A. Krasnow, D. W. Bianchi, E. E. Morrisey, B. L. Hogan, J. M. Kurie, D. C. Walker, D. C. Radisky, S. L. Nishimura, S. M. Violette, P. W. Noble, S. D. Shapiro, C. J. Blaisdell, H. A. Chapman, J. Kiley, D. Gail, D. Hoshizaki, Cell plasticity in lung injury and repair: Report from an NHLBI workshop, April 19-20, 2010. *Proc. Am. Thorac. Soc.* **8**, 215–222 (2011).
50. H. Chen, K. Matsumoto, B. L. Brockway, C. R. Rackley, J. Liang, J. H. Lee, D. Jiang, P. W. Noble, S. H. Randell, C. F. Kim, B. R. Stripp, Airway epithelial progenitors are region specific and show differential responses to bleomycin-induced lung injury. *Stem Cells* **30**, 1948–1960 (2012).
51. B. D. Singer, J. R. Mock, F. R. D'Alessio, N. R. Aggarwal, P. Mandke, L. Johnston, M. Damarla, Flow-cytometric method for simultaneous analysis of mouse lung epithelial, endothelial, and hematopoietic lineage cells. *Am. J. Physiol. Lung Cell. Mol. Physiol.* **310**, L796–L801 (2016).
52. Z. Borok, Alveolar epithelium: Beyond the barrier. *Am. J. Respir. Cell Mol. Biol.* **50**, 853–856 (2014).
53. T. S. Blackwell, A. M. Tager, Z. Borok, B. B. Moore, D. A. Schwartz, K. J. Anstrom, Z. Bar-Joseph, P. Bitterman, M. R. Blackburn, W. Bradford, K. K. Brown, H. A. Chapman, H. R. Collard, G. P. Cosgrove, R. Deterding, R. Doyle, K. R. Flaherty, C. K. Garcia, J. S. Hagood, C. A. Henke, E. Herzog, C. M. Hogaboam, J. C. Horowitz, T. E. King Jr., J. E. Loyd, W. E. Lawson, C. B. Marsh, P. W. Noble, I. Noth, D. Sheppard, J. Olsson, L. A. Ortiz, T. G. O'Riordan, T. D. Oury, G. Raghu, J. Roman, P. J. Sime, T. H. Sisson, D. Tschumperlin, S. M. Violette, T. E. Weaver, R. G. Wells, E. S. White, N. Kaminski, F. J. Martinez, T. A. Wynn, V. J. Thannickal, J. P. Eu, Future directions in idiopathic pulmonary fibrosis research. An NHLBI workshop report. *Am. J. Respir. Crit. Care Med.* **189**, 214–222 (2014).
54. N. Sakai, A. M. Tager, Fibrosis of two: Epithelial cell-fibroblast interactions in pulmonary fibrosis. *Biochim. Biophys. Acta* **1832**, 911–921 (2013).
55. M. Selman, A. Pardo, Role of epithelial cells in idiopathic pulmonary fibrosis: From innocent targets to serial killers. *Proc. Am. Thorac. Soc.* **3**, 364–372 (2006).
56. R. P. Naikawadi, S. Disayabutr, B. Mallavia, M. L. Donne, G. Green, J. L. La, J. R. Rock, M. R. Looney, P. J. Wolters, Telomere dysfunction in alveolar epithelial cells causes lung remodeling and fibrosis. *JCI Insight.* **1**, e86704 (2016).
57. S. Y. Pai, B. R. Logan, L. M. Griffith, R. H. Buckley, R. E. Parrott, C. C. Dvorak, N. Kapoor, I. C. Hanson, A. H. Filipovich, S. Jyonouchi, K. E. Sullivan, T. N. Small, L. Burroughs, S. Skoda-Smith, A. E. Haight, A. Grizzle, M. A. Pulsipher, K. W. Chan, R. L. Fuleihan, E. Haddad, B. Loechelt, V. M. Aquino, A. Gillio, J. Davis, A. Knutsen, A. R. Smith, T. B. Moore, M. L. Schroeder, F. D. Goldman, J. A. Connelly, M. H. Porteus, Q. Xiang, W. T. Shearer,

T. A. Fleisher, D. B. Kohn, J. M. Puck, L. D. Notarangelo, M. J. Cowan, R. J. O'Reilly, Transplantation outcomes for severe combined immunodeficiency, 2000-2009. *N. Engl. J. Med.* **371**, 434–446 (2014).
58. Y. Reisner, N. Kapoor, D. Kirkpatrick, M. S. Pollack, S. Cunningham-Rundles, B. Dupont, M. Z. Hodes, R. A. Good, R. J. O'Reilly, Transplantation for severe combined immunodeficiency with HLA-A, B, D, DR incompatible parental marrow cells fractionated by soybean agglutinin and sheep red blood cells. *Blood* **61**, 341–348 (1983).
59. A. M. Ferrazza, A. Gigante, M. L. Gasperini, R. M. Ammendola, G. Paone, I. Carbone, E. Rosato, Assessment of interstitial lung disease in systemic sclerosis using the quantitative CT algorithm CALIPER. *Clin. Rheumatol.* **39**, 1537–1542 (2020).
60. H. J. Park, S. M. Lee, J. W. Song, S. M. Lee, S. Y. Oh, N. Kim, J. B. Seo, Texture-based automated quantitative assessment of regional patterns on initial CT in patients with idiopathic pulmonary fibrosis: Relationship to decline in forced vital capacity. *AJR Am. J. Roentgenol.* **207**, 976–983 (2016).
61. T. Parimon, C. Yao, B. R. Stripp, P. W. Noble, P. Chen, Alveolar epithelial type II cells as drivers of lung fibrosis in idiopathic pulmonary fibrosis. *Int. J. Mol. Sci.* **21**, 2269 (2020).
62. T. H. Sisson, M. Mendez, K. Choi, N. Subbotina, A. Courey, A. Cunningham, A. Dave, J. F. Engelhardt, X. Liu, E. S. White, V. J. Thannickal, B. B. Moore, P. J. Christensen, R. H. Simon, Targeted injury of type II alveolar epithelial cells induces pulmonary fibrosis. *Am. J. Respir. Crit. Care Med.* **181**, 254–263 (2010).
63. A. Serrano-Mollar, M. Nacher, G. Gay-Jordi, D. Closa, A. Xaubet, O. Bulbena, Intratracheal transplantation of alveolar type II cells reverses bleomycin-induced lung fibrosis. *Am. J. Respir. Crit. Care Med.* **176**, 1261–1268 (2007).
64. A. Serrano-Mollar, G. Gay-Jordi, R. Guillamat-Prats, D. Closa, F. Hernandez-Gonzalez, P. Marin, F. Burgos, J. Martorell, M. Sanchez, P. Arguis, D. Soy, J. M. Bayas, J. Ramirez, T. D. Tetley, L. Molins, J. P. de la Bellacasa, C. Rodriguez-Villar, I. Rovira, J. J. Fibla, A. Xaubet, G. Pneumocyte Study, Safety and tolerability of alveolar type II cell transplantation in idiopathic pulmonary fibrosis. *Chest* **150**, 533–543 (2016).
65. Y. Wang, Z. Meng, M. Liu, Y. Zhou, D. Chen, Y. Zhao, T. Zhang, N. Zhong, X. Dai, S. Li, W. Zuo, Autologous transplantation of $P63^{+}$ lung progenitor cells for chronic obstructive pulmonary disease therapy. *Sci. Transl. Med.* **16**, eadi3360 (2024).
66. C. Hillel-Karniel, C. Rosen, I. Milman-Krentsis, R. Orgad, E. Bachar-Lustig, E. Shezen, Y. Reisner, Multi-lineage lung regeneration by stem cell transplantation across major genetic barriers. *Cell Rep.* **30**, 807–819.e4 (2020).
67. E. F. Redente, K. M. Jacobsen, J. J. Solomon, A. R. Lara, S. Faubel, R. C. Keith, P. M. Henson, G. P. Downey, D. W. Riches, Age and sex dimorphisms contribute to the severity of bleomycin-induced lung injury and fibrosis. *Am. J. Physiol. Lung Cell. Mol. Physiol.* **301**, L510–L518 (2011).
68. T. Ashcroft, J. M. Simpson, V. Timbrell, Simple method of estimating severity of pulmonary fibrosis on a numerical scale. *J. Clin. Pathol.* **41**, 467–470 (1988).
69. J. Clukers, M. Lanclus, B. Mignot, C. Van Holsbeke, J. Roseman, S. Porter, E. Gorina, E. Kouchakji, K. E. Lipson, W. De Backer, J. De Backer, Quantitative CT analysis using functional imaging is superior in describing disease progression in idiopathic pulmonary fibrosis compared to forced vital capacity. *Respir. Res.* **19**, 213 (2018).
70. D. J. Prockop, S. Udenfriend, A specific method for the analysis of hydroxyproline in tissues and urine. *Anal. Biochem.* **1**, 228–239 (1960).
71. T. K. McGovern, A. Robichaud, L. Fereydoonzad, T. F. Schuessler, J. G. Martin, Evaluation of respiratory system mechanics in mice using the forced oscillation technique. *J. Vis. Exp.* **75**, e50172 (2013).
72. A. Robichaud, L. Fereydoonzad, S. L. Collins, J. M. Loube, Y. Ishii, M. R. Horton, J. G. Martin, W. Mitzner, Airway compliance measurements in mouse models of respiratory diseases. *Am. J. Physiol. Lung Cell. Mol. Physiol.* **321**, L204–L212 (2021).
73. R. Satija, J. A. Farrell, D. Gennert, A. F. Schier, A. Regev, Spatial reconstruction of single-cell gene expression data. *Nat. Biotechnol.* **33**, 495–502 (2015).
74. A. Butler, P. Hoffman, P. Smibert, E. Papalexi, R. Satija, Integrating single-cell transcriptomic data across different conditions, technologies, and species. *Nat. Biotechnol.* **36**, 411–420 (2018).
75. S. Hanzelmann, R. Castelo, J. Guinney, GSVA: Gene set variation analysis for microarray and RNA-seq data. *BMC Bioinformatics* **14**, 7 (2013).
76. A. Liberzon, C. Birger, H. Thorvaldsdottir, M. Ghandi, J. P. Mesirov, P. Tamayo, The molecular signatures database hallmark gene set collection. *Cell Syst.* **1**, 417–425 (2015).
77. J. C. Schupp, T. S. Adams, C. Cosme Jr., M. S. B. Raredon, Y. Yuan, N. Omote, S. Poli, M. Chioccioli, K. A. Rose, E. P. Manning, M. Sauler, G. DeIuliis, F. Ahangari, N. Neumark, A. C. Habermann, A. J. Gutierrez, L. T. Bui, R. Lafyatis, R. W. Pierce, K. B. Meyer, M. C. Nawijn, S. A. Teichmann, N. E. Banovich, J. A. Kropski, L. E. Niklason, D. Pe'er, X. Yan, R. J. Homer, I. O. Rosas, N. Kaminski, Integrated single-cell atlas of endothelial cells of the human lung. *Circulation* **144**, 286–302 (2021).
78. M. Guo, M. P. Morley, C. Jiang, Y. Wu, G. Li, Y. Du, S. Zhao, A. Wagner, A. C. Cakar, M. Kouril, K. Jin, N. Gaddis, J. A. Kitzmiller, K. Stewart, M. C. Basil, S. M. Lin, Y. Ying, A. Babu, K. A. Wikenheiser-Brokamp, K. S. Mun, A. P. Naren, G. Clair, J. N. Adkins, G. S. Pryhuber, R. S. Misra, B. J. Aronow, T. L. Tickle, N. Salomonis, X. Sun, E. E. Morrisey, J. A. Whitsett; NHLBI LungMAP Consortium, Y. Xu, Guided construction of single cell reference for human and mouse lung. *Nat. Commun.* **14**, 4566 (2023).

Acknowledgments: We thank S. Schwarzbaum for critical reading of the manuscript. Y.R. is a CPRIT Scholar in Cancer Research in Houston, TX, USA. **Funding:** This study was supported in part by a grant from the Cancer Prevention and Research Institute of Texas (CPRIT RR170008), staff appreciation and recognition reward (STARs award from the UT system), the NIH/NHLBI under award number R01 HL129795 to B.F.D. and R01HL157100 and R01HL138510 to H.K.-Q., and the NIH/NCI under award number P30CA016672. **Author contributions:** Conceptualization: I.M.K., Y.R., and B.F.D. Methodology: I.M.K., Y.Z., C.R., E.Sho., S.Y.S, E.B.L., E.She., Y.R., H.K.Q., and B.F.D. Investigation: I.M.K., Y.Z., C.B., S.K.Y., C.R., E.Sho., E.She., S.Y.S., H.K.Q and Y.R. Formal analysis: J.W., Y.Q., Y.R., Y.Z., H.K.Q., and I.M.K. Visualization: I.M.K., Y.Z., J.W., Y.Q., and Y.R. Software: Y.Q. Data curation: Y.R., and I.M.K. Validation: Y.R., Y.Z., C.R., and I.M.K. Resources: Y.R., and H.K.Q. Funding acquisition: Y.R., H.K.Q., and B.F.D. Project administration: E.Sho., Y.R., H.K.Q., and I.M.K. Supervision: Y.R., H.K.Q., and I.M.K. Writing—original draft: Y.R. and I.M.K. Writing—review and editing: I.M.K., Y.R., S.Y.S., H.K.Q., and B.F.D. **Competing interests:** I.M.K., Y.Z., and Y.R. are inventors on US provisional patent application no. 63/441,122, submitted by MD Anderson Cancer Center and issued in 2023. The other authors declare that they have no competing interests. **Data and materials availability:** All data needed to evaluate the conclusions in the paper are present in the paper and/or the Supplementary Materials.

Submitted 10 August 2023
Accepted 19 July 2024
Published 23 August 2024
10.1126/sciadv.adk2524